Bioorganic & Medicinal Chemistry 21 (2013) 496–507

Contents lists available at SciVerse ScienceDirect

Bioorganic & Medicinal Chemistry

journal homepage: www.elsevier.com/locate/bmc

Fluorinated quinazolinones as potential radiotracers for imaging kinesin spindle protein expression

Jason P. Holland [a,b,*], Michael W. Jones [c], Susan Cohrs [d], Roger Schibli [b,d], Eliane Fischer [d,*]

[a] Division of Nuclear Medicine and Molecular Imaging, Massachusetts General Hospital, Department of Radiology, Harvard Medical School, 55 Fruit St., White 427, Boston, MA 02114, United States
[b] Institute of Pharmaceutical Sciences, ETH Zurich, Wolfgang-Pauli-Strasse 10, CH-8093, Zurich, Switzerland
[c] Chemistry Research Laboratory, 12 Mansfield Road, Oxford, OX1 3TA, United Kingdom
[d] Center for Radiopharmaceutical Sciences, Paul Scherrer Institute, Villigen, Switzerland

ARTICLE INFO

Article history:
Received 3 September 2012
Revised 24 October 2012
Accepted 6 November 2012
Available online 24 November 2012

Keywords:
Quinazolinone
Kinesin spindle protein
Mitosis
Fluorine
Allosteric inhibitors

ABSTRACT

Anti-mitotic anti-cancer drugs offer a potential platform for developing new radiotracers for imaging proliferation markers associated with the mitosis-phase of the cell-cycle. One interesting target is kinesin spindle protein (KSP)—an ATP-dependent motor protein that plays a vital role in bipolar spindle formation. In this work we synthesised a range of new fluorinated-quinazolinone compounds based on the structure of the clinical candidate KSP inhibitor, ispinesib, and investigated their properties in vitro as potential anti-mitotic agents targeting KSP expression. Anti-proliferation (MTT and BrdU) assays combined with additional studies including fluorescence-assisted cell sorting (FACS) analysis of cell-cycle arrest confirmed the mechanism and potency of these biphenyl compounds in a range of human cancer cell lines. Additional studies using confocal fluorescence microscopy showed that these compounds induce M-phase arrest via monoaster spindle formation. Structural studies revealed that compound **20**-(***R***) is the most potent fluorinated-quinazolinone inhibitor of KSP and represents a suitable lead candidate for further studies on designing ^{18}F-radiolabelled agents for positron-emission tomography (PET).

1. Introduction

Disruption of the normal processes that lead to cellular division during mitosis and subsequent induction of cell-cycle arrest and/or apoptosis is a key strategy in the design of modern chemotherapeutic agents for use in treating cancer. Indeed, the efficacy of many anti-cancer drugs used in the clinic relies on passive targeting of the hyper-proliferation status (increased rate of cellular division) of tumour versus normal tissues.[1]

Early development of anti-mitotic drugs focused on designing agents that bind to microtubules (MTs) and inhibit the normal function of the bipolar spindle. For example, common drugs which interfere with the dynamic instability of microtubules by forming either stabilising or destabilising interactions include taxanes (paclitaxel), *Vinca* alkaloids and epothilones. However, in the clinic use of these MT-targeted agents is often associated with severe side-effects such as peripheral neuropathy, which limits the maximum administered dose and duration of treatment.[1] More recently, as our knowledge of the cell cycle has evolved, the number and type of targets amenable for designing new anti-mitotic agents has grown exponentially.[2]

Over the last decade, kinesin motor proteins, such as kinesin spindle protein (KSP; kinesin-5; Eg5; KIF11) have emerged as potential targets for anti-mitotic drug development. Kinesins are a superfamily of motor proteins that typically use the energy derived from ATP-hydrolysis to generate force and/or transport cargo around the cell using the MT network.[3] KSP is a microtubule-associated homodimeric motor protein that functions during mitosis and is required for centrosome separation, bipolar spindle formation, proper segregation of sister chromatids and regulation of the rate of mitosis.[4] Modulation of the activity of KSP by immunodepletion of KSP protein, knockdown of KSP protein synthesis by using siRNA, or specific KSP inhibition using small-molecule agents like monastrol and ispinesib is known induce mitosis-phase (M-phase) arrest followed by apoptosis in either the M-phase (via mitotic catastrophe) or G_1-phase of the cell-cycle.[5–7]

In their landmark paper, Mayer et al.[8] demonstrated that inhibition of KSP using the small-molecule inhibitor monastrol induced a unique cellular phenotype in which the bipolar spindle formation fails due to improper separation of the centrosomes resulting in a characteristic monopolar (monoaster) spindle.[8,9] Subsequent structural and mechanistic studies revealed that monastrol inhibits

* Corresponding authors. Tel.: +1 617 726 6107; fax: +1 617 726 6165 (J.P.H.); tel.: +41 56 310 2857; fax: +41 56 310 2849 (E.F.).
E-mail addresses: holland.jason@mgh.harvard.edu (J.P. Holland), eliane.fischer@psi.ch (E. Fischer).

0968-0896/$ - see front matter © 2012 Elsevier Ltd. All rights reserved.
http://dx.doi.org/10.1016/j.bmc.2012.11.013

KSP by binding an allosteric site ~12 angstroms away from to the ATP-binding pocket.[10,11] Further chemical screening for novel pharmacophores specific for KSP inhibition led to the identification of numerous classes of structurally diverse compounds including the potent quinazolinone-based compound, ispinesib which has been evaluated in numerous Phase I and II clinical trials (Fig. 1).[12–15]

In our efforts toward developing radiolabelled agents for use in positron-emission tomography (PET) imaging of cancer, we reasoned that a radiotracer targeting KSP has the potential to inform medicinal chemists about drug transport, targeting and delivery, and could also provide a novel strategy for imaging tumour proliferation status by targeting cells in the M-phase. In this work we present details of the synthesis and preliminary in vitro evaluation of fluorinated quinazolinone derivatives based on the structure of ispinesib which have potential to be radiolabelled with fluorine-18 for developing new PET radiotracers.

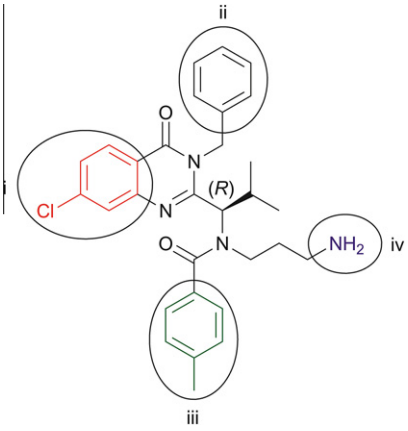

Figure 2. Diagram showing the potential sites for synthesising fluorinated quinazolinone derivatives of ispinesib which are potentially amenable to common ^{18}F-radiolabelling strategies. Substitution sites (i–iv) are discussed in the main text.

2. Results and discussion

2.1. Compound design

In designing a potential ^{18}F-radiopharmaceutical based the quinazolinone pharmacophore of ispinesib, we considered four possible locations for introducing the fluorine substituent (Fig. 2): (i) substitution of the Cl group on the quinazolinone ring, (ii) functionalisation of the benzyl group, (iii) replacement of the methyl substituent of the *para*-methylbenzamide group, and (iv) derivatisation of the free primary amino group. As ^{18}F is most commonly available as a nucleophilic source and the majority of ^{18}F-radiolabelling protocols employ nucleophilic substitution reactions,[16] it was important for our synthetic route to be amenable to incorporation of a suitable leaving group (in this case, NO_2).

Replacement of the Cl group of the quinazolinone ring with F or NO_2 (for synthesis of a precursor molecule suitable for radiolabelling) is feasible (Figure 2, position i). However, synthesis was prohibited by solubility issues as well as limited availability of sufficient starting materials (data not shown). In addition, introduction of a functional group modification at the first synthetic step is less desirable than at a late-stage. Functionalisation of the benzyl moiety (position ii) is feasible. Yet when considering subsequent ^{18}F-radiolabelling via an S_NAr reaction, the electron rich, non-activated aromatic ring is likely to hinder efficient substitution of a leaving group with ^{18}F anions.[16] Examination of the crystal structure of ispinesib bound in the allosteric pocket of KSP also revealed that functionalisation of the benzyl group would likely induce a loss of binding affinity due to steric interactions with the protein.[14] Based on crystallographic data, and structure-activity relations, functionalisation of the *para*-methylbenzamide group (position iii) or the free primary amine which is solvent exposed (position iv) is also feasible. Since ^{18}F-radiolabelling of the primary amine would require substantial structural modification involving the use of a radiolabelled prosthetic group such as amide coupling to [^{18}F]-SFB,[17] we elected to modify the *para*-methylbenzamide group in the synthesis of our fluorinated-derivatives.

Functionalisation of the *para*-methylbenzamide group has four distinct advantages. First, the aromatic ring in position iii is deactivated due to the electron withdrawing amide substituent which would facilitate S_NAr reactions for nucleophilic incorporation of ^{18}F. Second, the F and NO_2 derivatives can be introduced at a late-stage in the synthesis. Third, introducing fluorine in the *ortho*-, *meta*- and *para*-positions requires changing only one synthetic step and facilitates the study of structure-activity relationships. Fourth, it has been demonstrated that substitution of the methyl group for Br in CK-0106023 (Figure 1) does not interfere with the specificity or affinity of this compound for KSP.[9]

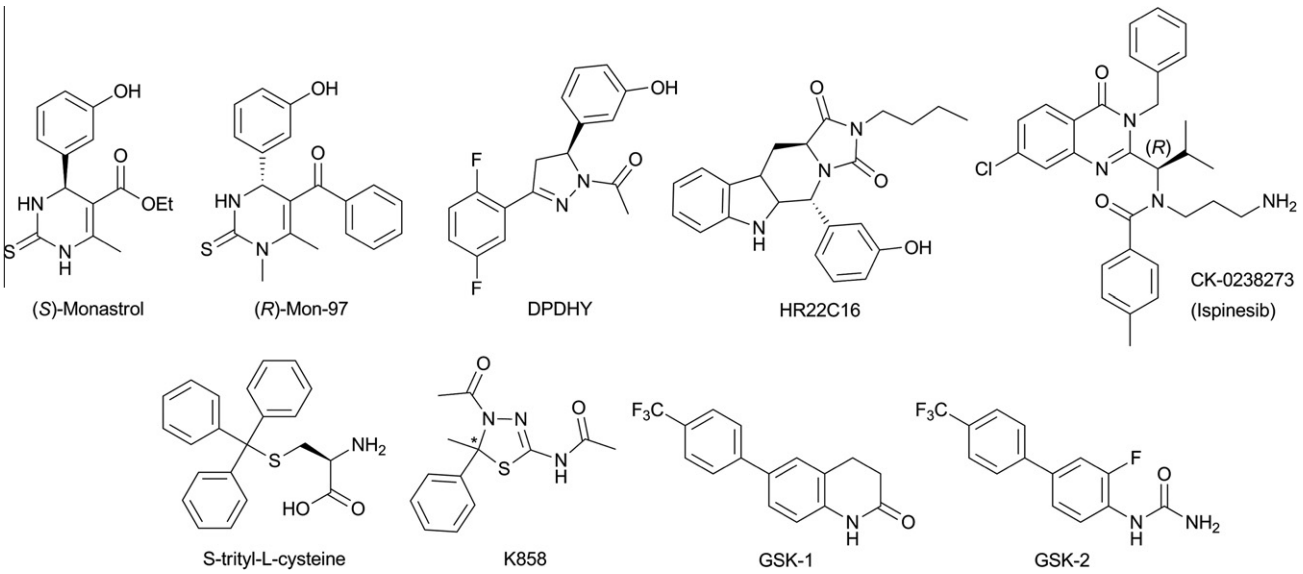

Figure 1. Structures of selected allosteric KSP inhibitors.

2.2. Chemical synthesis

The optimised synthesis of enantiomerically pure compounds **19**–**22** was accomplished in 11 steps in accordance with Scheme 1. Full synthetic details and characterisation data are given in the Section 4 (vide infra). Where appropriate, the structural identity and purity of all novel compounds has been characterised by using a range of experimental techniques including thin-layer chromatography (TLC), ^{1}H, $^{13}C\{1H\}$ and ^{19}F NMR spectroscopy, polarimetry and high resolution electrospray ionisation mass spectrometry.

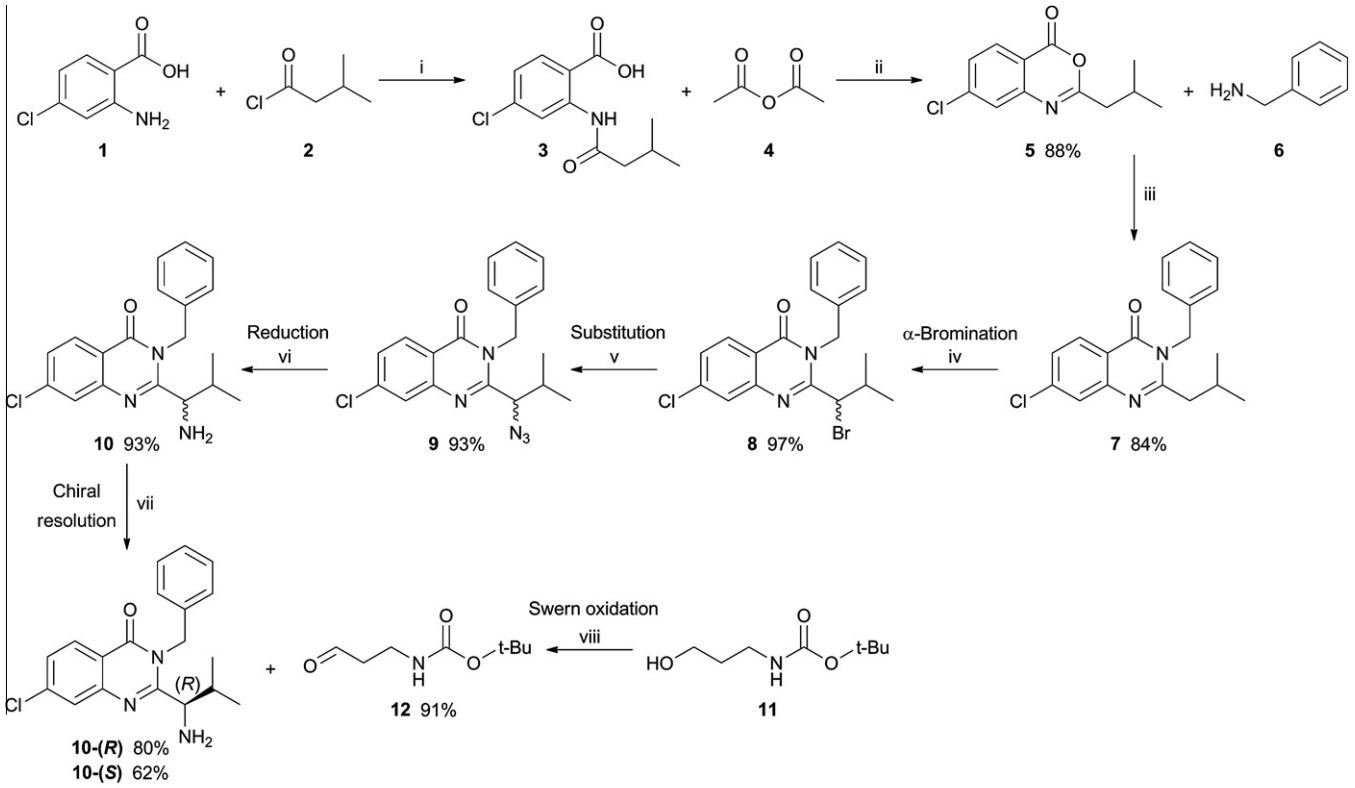

	R1	Yield / % (±)	(R)	(S)
14	p-CH_3	90%	92%	87%
15	p-F	85%	73%	81%
16	m-F	63%	74%	71%
17	o-F	89%	83%	69%
18	p-NO_2	91%	87%	84%

	R1	Yield / % (±)	(R)	(S)
19	p-CH_3	88%	85%	87%
20	p-F	81%	81%	85%
21	m-F	80%	89%	79%
22	o-F	81%	82%	74%

Scheme 1. Reaction scheme for the synthesis of quinazolinone compounds **14**–**22**. Reagents and conditions: (i) Compounds **1** and **2**, THF, stir, N_2(g), rt, 2 h, (ii) Crude intermediate **3**, acetic anhydride **4**, stir, N_2(g), 100 °C, 5 h, (iii) Compounds **5** and **6**, toluene, Dean–Stark reflux, N_2(g), 3 h, then add ethylene glycol and continue Dean–Stark reflux, 5 h, (iv) Compound **7**, NaOAc, glacial acetic acid, Br_2/acetic acid (dropwise) over 30 min, then stir, 45 °C, 4 h, (v) Compound **8**, NaN_3, anhydrous DMF, stir, 45 °C, 5 h, (vi) Compound **9**, EtOAc/MeOH (30 mL/100 mL), NH_4Cl(s), activated Zn(s) powder, stir, 60 °C, 30 min, (vii) Chiral resolution: for **10**-(***R***): Racemate **10**, (*R*,*R*)-(+)-2,3-dibenzyl-D-tartaric acid, propan-2-ol, stir, 85 °C, then cool to rt, 18 h. For **10**-(***S***) the same procedure was employed using (*S*,*S*)-(−)-2,3-dibenzyl-L-tartaric acid, (viii) Swern oxidation, oxalyl chloride, anhydrous DCM, DMSO, stir, Ar(g), −78 °C, then alcohol **11** (dropwise), −78 °C, followed by NEt_3, −78 °C to rt over 1 h, (ix) Compounds **10** and **12**, $NaBH(OAc)_3$, 1,2-dichloroethane, stir, Ar(g), rt, 6 h, (x) BOC-protected derivatives **14**–**18**: Compound **13** and substituted benzoyl chlorides (R_1 = p-CH_3, p-F, m-F, o-F, p-NO_2), DIPEA, anhydrous DCM, stir, rt, 24 h, (xi) BOC-deprotection: Compound **14**–**18**, trifluoroacetic acid, DCM, stir, N_2(g), rt, 2 h.

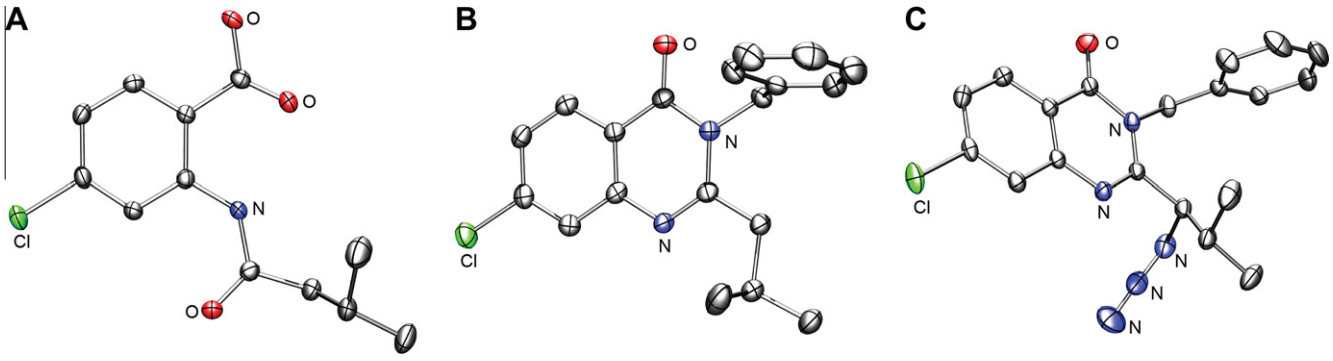

Figure 3. Representative images of the single crystal X-ray diffraction structures of (A) intermediate **3**, (B) compound **7** and (C) compound **9**. Thermal ellipsoids are shown at 50% probability. Hydrogen atoms have been omitted for clarity.

Compound **5** was isolated in 88% yield from a two-step reaction via intermediate **3** starting from 4-chloroanthranilic acid **1** and isovaleryl chloride **2**. Although isolation of intermediate **3** is possible and single crystals of **3** were obtained (Fig. 3A), reaction of the crude material with acetic anhydride proceeded in high yield. Reaction of compound **5** with benzyl amine under Dean–Stark reflux conditions afforded compound **7** in 84% yield. Then α-bromination followed by nucleophilic substitution with sodium azide gave compounds **8** and **9**, respectively. Single-crystal X-ray structures of key cyclized quinazolinone compound **7** and the racemic azide compound **9** are shown in Figure 3B and C, respectively. The azide group of compound **9** was subsequently reduced to a primary amine by using Zn/NH_4Cl to give racemate **10** in near quantitative yield over 3 steps from compound **7**.

Chiral resolution of **10** using enantiomers of 2,3-dibenzyl-D-tartaric acids, afforded enantiomerically pure compounds **10-(*R*)** and **10-(*S*)**. The absolute configuration of the chiral centre, and enantiomeric purity of compound **10-(*R*)** and **10-(*S*)** was confirmed after synthesising the Mosher's amide derivatives **23-(*R*,*R*)** and **23-(*R*,*S*)** (Scheme 2). ^{1}H NMR analysis was conducted in accordance with the methods described by Hoye et al.[18] Both compounds **23-(*R*,*R*)** and **23-(*R*,*S*)** were obtained in greater than 99% de, confirming the enantiomeric purity of the parent compounds **10-(*R*)** and **10-(*S*)**.

Following the Swern oxidation of compound **11**, and the reductive amination of compound **10** in the presence of compound **12** and $NaBH(OAc)_3$ furnished compound **13** in ~75% yield. Here, compound **13** was used as a common intermediate for all derivatives, thus minimising the number of synthetic steps required after introducing the different substituents. Notably, introduction of the *para*-nitro substituent in the BOC-protected compound **18** occurs as the final step for the synthesis of the ^{18}F-radiolabelling precursor. Finally, deprotection using trifluoroacetic acid yielded compounds **19–22** in overall yields ranging from 21% to 38% over a total of 10 or 11 steps. Compounds **19–22** were evaluated for their potential to inhibit KSP by using a range of protein and cellular-based assays in vitro.

2.3. Kinesin motor protein inhibition assays

After successful isolation of the fluoro-quinazolinone derivatives **20–22**, we first investigated their ability to inhibit the enzymatic ATP-hydrolysis activity of KSP, as well as their selectivity for KSP versus a panel of diverse kinesin motor proteins (Table 1 and Supplementary data Fig. S1). Kinesins investigated included centromeric protein-E (CENP-E), mitotic centromere-associated kinesin (MCAK), kinesin heavy chain (KHC) and kinesin protein KIFC3. In addition, (*S*)-monastrol and (*R*)-ispinesib (**19-(*R*)**) were

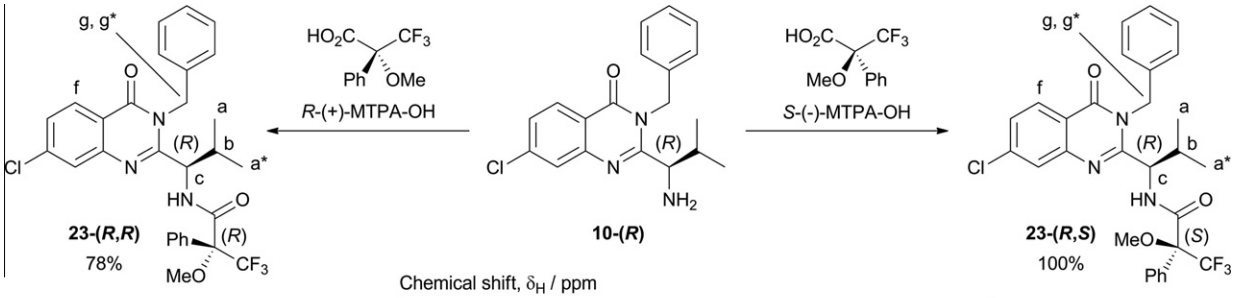

Resonance	Chemical shift, δ_H / ppm 23-(*R*,*R*)	23-(*R*,*S*)	Δ [δ(*R*,*S*) - δ(*R*,*R*)] / ppm	Δ [δ(*R*,*S*) - δ(*R*,*R*)] / Hz
a	0.3854	0.4446	0.0592	23.68
a*	0.7362	0.9101	0.1739	69.56
b	2.0864	2.1427	0.0563	22.5
c	5.1601	5.1286	-0.0315	-12.6
f	8.2790	8.2704	-0.0086	-3.46
g	5.2830	5.2389	-0.0440	-17.62
g*	5.8134	5.7667	-0.0467	-18.68

Scheme 2. Reaction scheme showing the synthesis and structures of Mosher's amides I and II derived from amide coupling of compound **10**-(***R***) with *R*-(+)-MTPA-OH or *S*-(−)-MTPA-OH to give compounds **23**-(***R*,*R***) and **23**-(***R*,*S***), respectively. ^{1}H NMR resonance assignments are presented (letters a–g) and chemical shift data are given in the table (inset). NB: Analysis and assignment of the absolute stereochemical configuration of compound **10**-(***R***) was accomplished in accordance with the methods of Hoye et al.[18] where R^1 = isopropyl group and R^2 = quinazolinone ring.

Table 1
Percentage of kinesin motor protein ATP-hydrolysis activity relative to untreated controls/%

Compound	Relative kinesin motor protein ATP-hydrolysis activity/%				
	KSP	CENP-E	MCAK	KHC	KIFC3
(*S*)-Monastrol (10 μM)	10.8 ± 1.4	97.7 ± 2.2	97 ± 2.1	98.5 ± 1.0	98.3 ± 2.6
19-(***R***) (1 μM)	8.8 ± 1.4	98 ± 3.7	96.7 ± 3.2	101.5 ± 4.3	97.3 ± 2.8
19-(***S***) (1 μM)	99.4 ± 1.1	99.1 ± 1.6	99.2 ± 2.3	96.8 ± 2.3	97.9 ± 2.5
20-(***R***) (1 μM)	2.7 ± 1.7	99.8 ± 1.6	99.2 ± 2.4	97.1 ± 3.3	101.3 ± 1.9
20-(***S***) (1 μM)	96.1 ± 2.6	97.4 ± 2.0	98.9 ± 1.8	99.2 ± 2.0	98.7 ± 1.9
21-(±) (1 μM)	10.1 ± 3.2	97.4 ± 1.9	96.4 ± 2.5	99.1 ± 2.1	99.4 ± 1.4
21-(***S***) (1 μM)	95.5 ± 3.0	100.5 ± 1.7	98.6 ± 1.2	98.9 ± 1.8	98.9 ± 1.8
22-(***R***) (1 μM)	7.5 ± 2.4	99.1 ± 1.7	98.7 ± 3.1	97.2 ± 3.2	99.4 ± 2.0
22-(***S***) (1 μM)	95.9 ± 3.4	97.9 ± 2.0	98.2 ± 2.1	97.9 ± 1.9	98.8 ± 2.1

Table 2
Data on the GI_{50} values for growth inhibition in four human cancer cell lines by compounds **20**–**22** as measured by using MTT assays

Compound	DU-145 cells			PC-3 cells			MCF-7 cells			SKOV-3 cells		
	$GI_{50}(1)/\mu M$[a]	$GI_{50}(2)/nM$[b]	R^2	$GI_{50}(1)/\mu M$	$GI_{50}(2)/nM$	R^2	$GI_{50}(1)/\mu M$	$GI_{50}(2)/nM$	R^2	$GI_{50}(1)/\mu M$	$GI_{50}(2)/nM$	R^2
20-(***R***)	2.2 ± 2.4	0.19 ± 0.1	0.968	5.1 ± 1.2	0.5 ± 0.1	0.933	2.5 ± 1.1	1.0 ± 0.2	0.946	15.4 ± 4.5	0.00226 ± 0.0004	0.967
20-(±)	3.1 ± 3.6	1.1 ± 0.1	0.958	6.3 ± 1.5	1.1 ± 0.3	0.938	2.7 ± 1.1	4.0 ± 0.6	0.969	4.3 ± 2.5	2.7 ± 0.6	0.932
20-(***S***)	0.35 ± 0.05	N/A[d]	0.953	1.3 ± 0.2	N/A	0.898	1.1 ± 0.2	N/A	0.958	0.5 ± 0.05	N/A	0.981
21-(±)	3.3 ± 14.9	4.0 ± 0.6	0.961	7.6 ± 2.8	17.0 ± 7.3	0.915	2.9 ± 1.4	5.1 ± 0.8	0.970	5.7 ± 3.2	15.6 ± 3.2	0.968
21-(***S***)	0.52 ± 0.09	N/A	0.918	1.8 ± 0.2	N/A	0.965	0.63 ± 0.12	N/A	0.898	1.1 ± 0.2	N/A	0.923
22-(***R***)	5.6 ± 17.8	10.7 ± 1.2	0.979	4.6 ± 1.5	7.8 ± 3.7	0.909	3.0 ± 1.3	4.2 ± 0.7	0.970	5.35 ± 6.4	34.8 ± 13.6	0.913
22-(±)	ND[c]	48.5 ± 7.5	0.945	0.35 ± 0.1	1.9 ± 0.8	0.961	1.9 ± 1.3	17.7 ± 3.6	0.971	3.1 ± 2.7	34.6 ± 9.5	0.960
22-(***S***)	0.72 ± 0.10	N/A	0.946	0.16 ± 0.02	N/A	0.942	2.0 ± 0.4	N/A	0.877	0.85 ± 0.12	N/A	0.946

NB: Where two separate GI_{50} values are given, a biphasic model was employed. For (*S*)-enantiomers a single value derived from monophasic non-linear regression analysis is given.

[a] GI_{50} value for non-specific cytotoxicity in μM.
[b] GI_{50} value for M-phase KSP inhibition of cell-cycle progression (cytostatis).
[c] Not determined.
[d] Not applicable.

used as positive controls, and the inactive stereoisomer (*S*)-ispinesib **19-(*S*)** was used as a negative chemical control for KSP inhibition.

These assays indicated that only the (*R*)-enantiomers of compounds **19**–**22** are active toward KSP inhibition in vitro. Further, the (*R*)-enantiomers of compounds **19**–**22** were found to be selective for KSP inhibition and failed to inhibit the ATP-hydrolysis activity of CENP-E, MCAK, KHC or KIFC3. Interestingly, structure-activity relations suggest that the fluorine atom can be located in the *ortho*-, *meta*- or *para*-position (Scheme 1) without compromising binding or selective inhibition of KSP.

2.4. Cellular growth inhibition assays

We next investigated the potency of the fluoro-compounds **20**–**22** toward cellular growth inhibition in DU-145 and PC-3 prostate cancer, MCF-7 breast cancer and SKOV-3 ovarian cancer cells (Table 2 and Fig. 4). Previous work on KSP inhibition has focused on the use of drugs like ispinesib to inhibit the growth of colorectal carcinomas (using HCT116 cells) and ovarian cancer (SKOV-3 cells).[9] These two cell lines were found to be particularly sensitive toward KSP inhibition. In this work, we were also interested in evaluating the potential scope of our novel quinazolinone compounds toward growth inhibition of different cancer cell lines.

Cell proliferation data indicate that after 44 h incubation, compounds **20**–**22** were found to inhibit growth of all four cell lines. The (*R*)-enantiomers of all compounds were most active, and in general, the *para*-fluoro derivative (compound **20**) was more potent than either the *meta*- or *ortho*-isomers (compounds **21** and **22**, respectively). Analysis of dose–response curves for treatment with the (*R*)-enantiomers or racemates showed a biphasic profile with non-linear regression analysis yielding two growth inhibition values centred in the micromolar ($GI_{50}(1)/\mu M$) and nanomolar ($GI_{50}(2)/nM$) concentration ranges (Figs. 4A and 5). For analysis of growth inhibition curves derived from cells treated with (*S*)-enantiomers, a monotonic sigmoid shape was used with non-linear regression analysis yielding one measure of growth inhibition ($GI_{50}(1)/\mu M$) in the micromolar range. At relatively high concentrations (typically >0.5–10 μM) all compounds were found to be cytotoxic. The mechanism of induced cell death is uncertain but is tentatively assigned to general cytotoxic effects from treatment with high concentrations of these agents. For the (*S*)-enantiomers, treatment with drug concentrations <0.1 μM did not affect cellular growth/proliferation with absorbance values corresponding to those measured for control (vehicle treated) samples. However, treatment with the (*R*)-enantiomers and racemates resulted in a dramatically different profile; below the cytotoxic threshold at concentrations in the range ~1 to ~10 nM, a plateau was observed. At concentrations below the plateau (<10 nM) we observed a second sigmoidal profile with measured absorbance increasing to that observed in vehicle-treated control samples. Non-linear regression analysis of this biphasic profile yielded $GI_{50}(2)/nM$ values in the nanomolar range (Table 2 and Fig. 5). In the concentration range corresponding to the plateau between the $GI_{50}(1)$ and $GI_{50}(2)$ values, (*R*)-enantiomers of compounds **20**–**22** likely inhibit cell-cycle progression by inducing cytostasis in the M-phase from KSP inhibition. It is plausible that at sub-nM concentrations, these drugs are not present in sufficiently high amounts to effectively inhibit all KSP motor protein present, and therefore, cell-cycle progression proceeds as in control samples.

Structure–activity relationships for growth inhibition studies showed the same trend of potency for all compounds tested in DU-145, PC-3 and MCF-7 cells. For each of these three cell lines, compound **20-(*R*)** was the most potent with $GI_{50}(2)$ values ranging from 0.19 nM (DU-145 cells) to 0.98 nM (MCF-7 cells). Our results also demonstrate that of the cancer cell lines tested, SKOV-3 cells

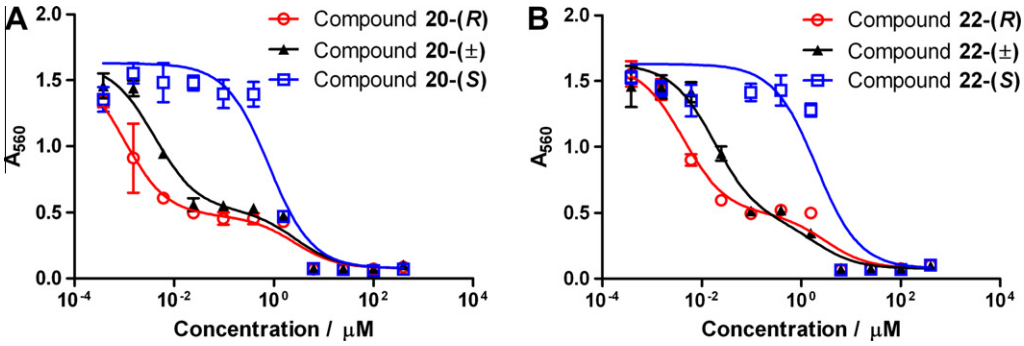

Figure 4. Representative growth inhibition curves showing the effect of enantiomerically pure and racemic mixtures on growth inhibition of MCF-7 breast cancer cells for (A) *para*-fluoro compound **20** and (B) *ortho*-fluoro compound **22**.

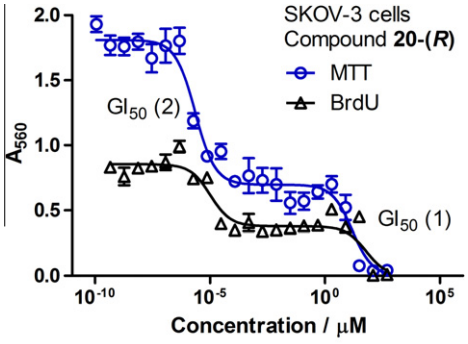

	GI_{50} (1) / μM	GI_{50} (2) / nM
MTT	15.35 ± 4.51	0.0023 ± 0.0004
BrdU	60.95 ± 27.13	0.0104 ± 0.0035

Figure 5. Detailed comparison of the biphasic growth inhibition profile observed in MTT and BrdU assays on treatment of SKOV-3 cells with compound **20**-(***R***).

are by far the most sensitive toward KSP inhibition with compound **20-(*R*)** (Fig. 5 and Table 2). MTT assays revealed that compound **20-(*R*)** has the same general cytotoxic value as the other compounds/isomers tested with $GI_{50}(1)$ = 15.4 ± 4.5 μM, but a significantly lower $GI_{50}(2)$ value for growth arrest of only 0.00226 ± 0.0004 nM in SKOV-3 cells. This pico-molar potency of compound **20-(*R*)** toward induced growth arrest in SKOV-3 cells was confirmed by using independent BrdU growth inhibition assays which gave $GI_{50}(1)$ and $GI_{50}(2)$ values of 61.0 ± 27.0 μM and 0.010 ± 0.004 nM, respectively. *NB: All assays were performed in quadruplicate to minimise contributions from irreproducible errors.* Overall, these results are consistent with previous reports which noted that SKOV-3 cells are particularly sensitive toward KSP inhibition with quinazolinone-based drugs.[9] At present, the reasons why SKOV-3 cells display such extreme sensitivity toward KSP inhibition with compounds **19-(*R*)** and **20-(*R*)** remain uncertain.

2.5. Cell-cycle analysis

In order to confirm that the anti-proliferative effects observed in the MTT and BrdU assays were the result of inhibition of cellular proliferation in the M-phase, we investigated changes in cell-cycle population numbers on treatment with the (*R*)- and (*S*)-enantiomers of the most potent new compound **20** by using fluorescence-assisted cell sorting (FACS; Fig. 6 and Table 3). The (*R*)- and (*S*)-enantiomers of ispinesib (compound **19**) were used as positive and negative chemical controls, respectively. Changes in DNA content, and hence, the number of cells associated with a given phase of the cell-cycle were measured by staining with propidium iodide (PI). In addition, we used immuno-staining of phospho-histone H3 (pH3), a specific marker of mitosis,[19] to deconvolute changes in the cell population numbers in the G_2/M-phase.

DNA content analysis demonstrated that (*S*)-enantiomers of compounds **19** and **20** do not affect the relative distribution of cells in the G_0/G_1, S and G_2/M-phases of the cell cycle (Fig. 6A). Further, treatment of cells with (*S*)-enantiomers at 100 nM concentration does not induce cell death as demonstrated by the absence of cells in the sub-G_1 population. In contrast, treatment with the active (*R*)-enantiomers of compounds **19** and **20** induced a dramatic shift in the population profiles. For both compounds, the number of cells found in the G_2/M-phase increased, with a concordant decrease in the G_0/G_1 phase. For instance, treatment of SKOV-3 cells with compound **20-(*R*)** induced an increase in the G2/M-phase population from 21.8% (vehicle) to 58.5% whereas for compound **20-(*S*)** the population remained at 22.5% (Table 3). Notably, FACS data for treatment with compounds **19-(*R*)** and **20-(*R*)** also showed an increase in the number of cells associated with the sub-G_1 population which is assigned to induced apoptosis (likely resulting from mitotic catastrophe). Similar results were found across all cell lines studied.

An increase in the G_2/M-phase population does not necessarily confirm the mechanism of inhibition. Therefore, we conducted pH3 staining to evaluate the contribution from cells in the M-phase (Figs. 6B and C). From the 2-dimensional scattergrams we observed that treatment of SKOV-3 cells with compound **20-(*R*)** resulted in 58.8% of cells associated with the M-phase. In contrast, treatment with compound **20-(*S*)** resulted in only 2.6% of cells in mitosis. These FACS data demonstrate that the anti-proliferative effects of (*R*)-quinazolinone-based agents are the result of induced M-phase arrest. Further, our data are consistent with the known mechanism of action of KSP inhibition with other inhibitors including monastrol, ispinesib and progenitor biphenyl compounds.[8,9,20]

2.6. Confocal fluorescence microscopy

After establishing the relative sensitivity of various human cancer cell lines toward treatment with compounds **20**–**22**, we next investigated the induced phenotypic effects by using confocal fluorescence microscopy. KSP is required for bipolar spindle formation and force generation on interpole MTs.[21] Inhibition of KSP induces M-phase arrest during prophase/prometaphase, which prevents separation of the two centrosome to opposite poles of the cell. Thus, KSP inhibition leads to a failure to establish a functional bipolar spindle, and gives rise to a characteristic monoaster phenotype.[8]

Human cancer cells were grown for 22 h on 8-well chambered microscope slides before treating with compounds **20**–**22** (100

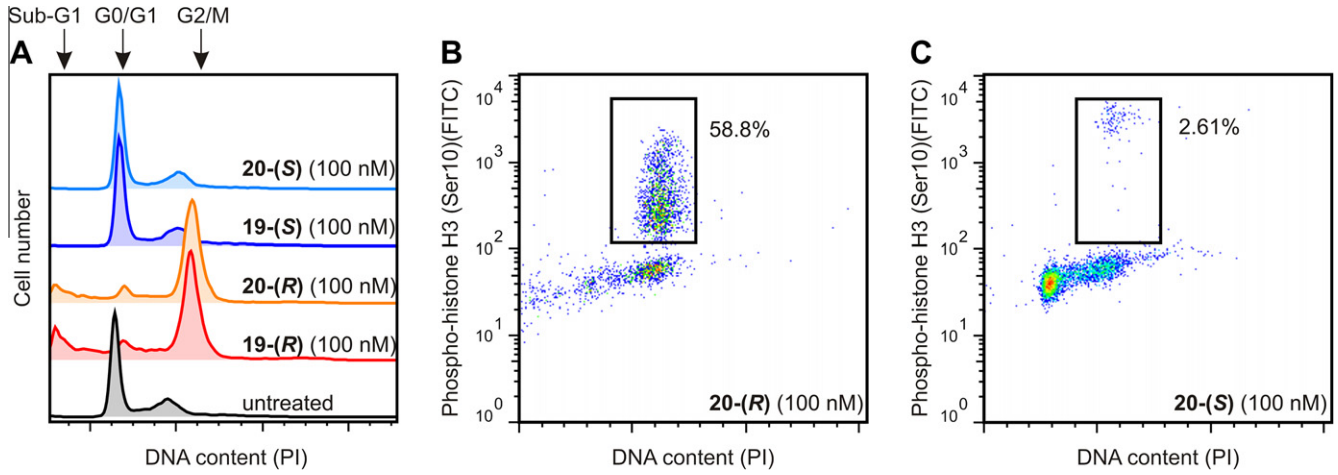

Figure 6. Representative cell-cycle analysis data derived from FACS studies on treatment of SKOV-3 cells with the (*R*)- and (*S*)-enantiomers of compounds **19** and **20**. (A) Stacked plot of 1-dimensional histograms showing the change in DNA content, hence shift in the percentage of cells found in the G_0/G_1, S and G_2/M phase of the cell-cycle between vehicle-treated control cells and cells treated with quinazolinone-based drugs (100 nM). PI = Propidium iodide. 2-Dimensional scattergrams showing the change in phospho-histone H3 (pH3) stained cells versus DNA content (PI staining) for (B) treatment with compound **20**-(***R***), and (C) treatment with compound **20**-(***S***).

Table 3
Data showing the measured percentage of cells in the G_1/G_0, S and G_2/M phases of the cell-cycle upon treatment with either vehicle (<1% DMSO in medium) or compounds **20**–**22** (100 nM) at 37 °C for 24 h

Compound	DU-145 cells			PC-3 cells			MCF-7 cells			SKOV-3 cells		
	G_0/G_1	S	G_2/M	G_0/G_1	S	G_2/M	G_0/G_1	S	G_2/M	G_0/G_1	S	G_2/M
Vehicle	53.2	4.5	31	32.6	14.2	26.3	48.2	19.6	22.4	51.1	18.4	21.8
19-(*R*)	24.8	10.8	49.8	13.8	10.1	60.9	22.1	10.6	57.2	3.8	13.6	51.3
19-(*S*)	53.7	10.3	24.5	34.4	30.0	25.0	49.7	17.6	21.2	49.8	16.6	14.5
20-(*R*)	ND [a]	ND	ND	12.0	11.1	63.6	25.1	12.0	53.2	3.5	13.8	58.5
20-(*S*)	52.9	9.5	27.7	31.0	24.2	32.9	51.3	15.2	22.8	51.9	16.2	22.5

[a] ND = Not determined.

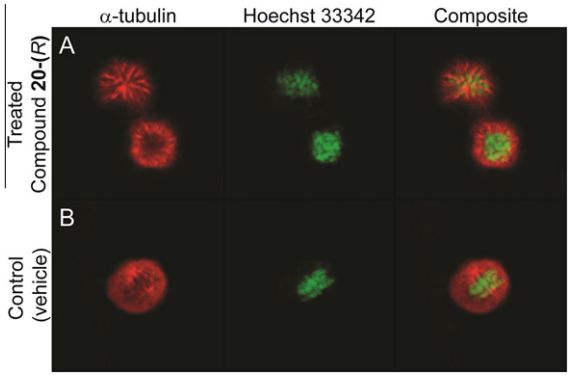

Figure 7. Representative confocal fluorescence microscopy images showing the effects of treatment of SKOV-3 cells with compound **20**-(***R***) at 100 nM after incubation at 37 °C for 22 h. (A) Two cells displaying monoaster MT spindle formation (red) and diffuse staining for DNA (green)—a characteristic phenotype indicative of KSP inhibition and M-phase arrest. (B) Representative images of a vehicle-treated SKOV-3 cell undergoing normal mitosis (anaphase). Full microscopy details are given in the Section 4.

nM) or vehicle (<1% DMSO in medium) at 37 °C for 24 h. SKOV-3 cells were then fixed and permeabilised before staining with an anti-α-tubulin antibody (and a secondary antibody labelled with Alexa Fluor 568) to probe the structure of the MT-network, and Hoechst 33342 to stain for DNA. Representative confocal fluorescence microscopy images showing the effect of treating SKOV-3 cells with compound **20**-(***R***) are presented in Figure 7.

In the control (vehicle-treated) SKOV-3 cells, we observed cells undergoing normal mitotic division with a well-defined bipolar spindle with chromosomes aligned on the metaphasic plate (Fig. 7B). In contrast, no cells in the normal stages of mitosis were identified after treatment with compound **20**-(***R***). Instead, we observed that the majority of treated cells exhibited a monoaster phenotype (Fig. 7A). Results were confirmed by using (*R*)-ispinesib and (*S*)-ispinesib as positive and negative controls, respectively (data not shown). Interestingly, after 22 h incubation virtually all SKOV-3 cells treated with (*R*)-enantiomers of compounds **20**–**22** displayed a monoaster phenotype. These data are congruent with the results obtained from anti-proliferative MTT and BrdU assays as well as from the FACS studies where we observed a biphasic growth inhibition profile and a plateau corresponding G_2/M-phase to cell-cycle arrest.

Taken together, our experimental data provide compelling evidence that the anti-proliferative effects of compounds **20**–**22** are consistent with the known mechanism of action of the parent drug ispinesib. Further, we conclude that introduction of the *para*-fluoro substituent in compound **20** is tolerated and does not adversely affect the specificity or potency of this compound toward KSP inhibition in vitro. Collectively, the results presented here provide strong support for the future development of an ^{18}F-radiolabelled analogue of compound **20**-(***R***) as a potential PET radiopharmaceutical for imaging KSP expression and monitoring tissue proliferation status in vivo.

3. Conclusions

Here we report the synthesis and in vitro characterisation of a range of fluorinated quinazolinone compounds based on the structure of ispinesib, a potent KSP inhibitor. Introduction of a fluorine

substituent in place of the methyl group of the *para*-methylbenzamide moiety of ispinesib was well-tolerated with compounds **20**–**22** retaining specificity and potency toward KSP protein inhibition and anti-proliferative activity in a range of human cancer cell lines. Structure-activity studies revealed that the *para*-fluoro isomer was generally more potent than the *meta*- or *ortho*-fluoro derivatives and represents a suitable lead compound for developing a novel ^{18}F-radiotracer for PET imaging of KSP expression and tissue proliferation status. Work on the radiosynthesis of [^{18}F]-**20**-(***R***) from the *para*-nitro precursor compound **18**-(***R***) is underway.

4. Experimental

Full details are reported in the Supplementary data.

4.1. Synthesis

Synthetic methods and characterization data for compounds **5**, **7**–**10**, **12** and **13** are presented in the Supplementary data.

4.1.1. General method A

BOC-protect derivatives of ispinesib were synthesised by using the same general method A given here for the synthesis of (±)-*tert*-butyl (3-(*N*-(1-(3-benzyl-7-chloro-4-oxo-3,4-dihydroquinazolin-2-yl)-2-methylpropyl)-4-methylbenzamido)propyl)carbamate, racemate **14**.

To a flame dried 25 mL round bottom flask was added compound **13** (0.15 g, 0.30 mmol), anhydrous dichloromethane (2.5 mL) and diisopropylethylamine (DIPEA; 0.097 g, 0.75 mmol, 2.5 equiv) in anhydrous dichloromethane (1 mL). Then *p*-toluoyl chloride (0.065 g, 0.42 mmol, 1.4 equiv) was dissolved in anhydrous dichloromethane (<2 mL) and added to the reaction which was subsequently stirred at rt for 24 h. Progress of the reaction was monitored by TLC (30% EtOAc/hexanes/~0.1% conc. NH_3, UV) with the product observed at R_f = 0.39. The reaction was quenched by pouring onto sat. $NaHCO_3$(aq) (30 mL), and extracted with dichloromethane (3 × 20 mL). The organic fractions were combined, washed with brine (1 × 30 mL), dried over Na_2SO_4(s) for 30 min, filtered and then the solvent was removed under reduced pressure. The extraction process removed several of the major impurities observed near the baseline by TLC analysis. The crude mixture was purified by using silica gel chromatography (15–20% EtOAc/hexane/~0.1% conc. NH_3). Fractions containing the product were identified by TLC, pooled and the solvent was removed under reduced pressure. Then the sample was dried in vacuo to give compound **14** as a white, microcrystalline solid (0.167 g, 0.27 mmol, 90%). ^{1}H NMR (400 MHz, $CDCl_3$): δ_H 0.36 (d, 3H, $^3J_{HH}$ = 6.4 Hz, magnetically inequivalent CH(CH_3)$_2$), 0.73–0.90 (m, 2H, –$CH_2CH_2CH_2$), 0.88 (d, 3H, $^3J_{HH}$ = 6.6 Hz, magnetically inequivalent CH(CH_3)$_2$), 1.41 (s, 9H, –OC(CH_3)$_3$), 2.38 (s, 3H, PhCH_3), 2.58–2.78 (m, 3H, overlapping resonances: 1H, $CH_2CH(CH_3)_2$, and 2H, $NCH_2CH_2CH_2$–), 3.33–3.51 (m, 2H, $NCH_2CH_2CH_2$–), 3.88 (br s, 1H, NHC(O)), 5.23 (d, 1H, $^2J_{HH}$ = 15.7 Hz, roofing diastereotopic PhCH_2), 5.70 (d, 1H, $^3J_{HH}$ = 10.6 Hz, $CHCH(CH_3)_2$), 6.12 (d, 1H, $^2J_{HH}$ = 15.7 Hz, roofing diastereotopic PhCH_2), 7.20 (s, 4H, 4 × Ar-CH, tolyl group), 7.26 (m, 2H, *o*-Ph overlapping with $CHCl_3$ residual solvent resonance), 7.31 (m, 1H, *p*-Ph), 7.40 (m, 2H, *m*-Ph), 7.49 (dd, 1H, $^3J_{HH}$ = 8.6 Hz and w-coupling $^4J_{HH}$ = 2.0 Hz, Ar: -CH-C*H*-C(Cl)CH-), 7.76 (d, 1H, w-coupling $^4J_{HH}$ = 2.0 Hz, Ar: CH–C(Cl)–C*H*C(N)), 8.32 (d, 1H, $^3J_{HH}$ = 8.6 Hz, Ar: C–C*H*–CH–C(Cl)). ^{13}C{^{1}H} (100 MHz, $CDCl_3$): δ_C 18.4 (CH_3), 19.3 (CH_3), 21.5 (PhCH_3), 28.5 (3 × CH_3), 29.0 ($CHCH(CH_3)_2$: HSQC), 30.9 (–$NCH_2CH_2CH_2$–), 37.8 (–$NCH_2CH_2CH_2$–), 42.1 (–$NCH_2CH_2CH_2$–), 45.7 (PhCH_2), 59.7 ($CHCH(CH_3)_2$), 79.4 (O$C(CH_3)_3$), 119.5 (IV° C), 126.1 (2C, Ar: 2 × CH_3CH), 127.0 (Ar: CH–C(Cl)–C*H*C(N)), 127.5 (2 × *o*-Ph), 127.8 (*p*-Ph), 128.3 (Ar: –CH–C*H*–C(Cl)CH–), 128.9 (2C, Ar: 2 × CH_3CHCH), 129.1 (Ar: –C*H*–CH–C(Cl)CH), 129.4 (2 × *m*-Ph), 133.9 (IV° C), 137.0 (IV° C), 139.7 (IV° C), 141.0 (IV° C), 147.7 (IV° C), 156.1 (IV° C), 162.3 (IV° C), 173.2 (IV° C). MS *m*/*z* (MeCN) 617 (100%) [M+H$^+$]. HRMS-ESI *m*/*z* (DCM/MeOH) found 617.2893, calcd for $C_{35}H_{42}ClN_4O_4$ 617.2889 [M+H$^+$]. $[\alpha]_D$ (25 °C; $CHCl_3$; **14-(*R*)**) = +269.7 ± 0.7. Analytical data for the synthesis of **14-(*R*)** and **14-(*S*)** were identical.

4.1.2. (*R*)-*tert*-Butyl (3-(*N*-(1-(3-benzyl-7-chloro-4-oxo-3,4-dihydroquinazolin-2-yl)-2-methylpropyl)-4-fluorobenzamido) propyl)carbamate 15-(*R*)

Compound **13-(*R*)** (0.150 g, 0.30 mmol) was reacted with *p*-fluorobenzoyl chloride (0.067 g, 0.42 mmol, 1.4 equiv) in accordance with general method A to give compound **15-(*R*)** as a white solid (0.135 g, 0.218 mmol, 73%). ^{1}H NMR (400 MHz, $CDCl_3$): δ_H 0.31 (d, 3H, $^3J_{HH}$ = 6.4 Hz, magnetically inequivalent CH(CH_3)$_2$), 0.74 (m, 1H, –$CH_2CH_2CH_2$ diastereotopic), 0.89 (d, 3H, $^3J_{HH}$ = 6.7 Hz, magnetically in equivalent CH(CH_3)$_2$), 1.11 (m, 1H, –$CH_2CH_2CH_2$ diastereotopic), 1.35 (s, 9H, –OC(CH_3)$_3$), 2.53–2.73 (m, 3H, overlapping resonances: 1H, $CH_2CH(CH_3)_2$, and 2H, $NCH_2CH_2CH_2$–), 3.25–3.48 (m, 2H, $NCH_2CH_2CH_2$–), 3.97 (br s, 1H, NHC(O)), 5.16 (d, 1H, $^2J_{HH}$ = 15.7 Hz, roofing diastereotopic PhCH_2), 5.64 (d, 1H, $^3J_{HH}$ = 10.6 Hz, $CHCH(CH_3)_2$), 6.06 (d, 1H, $^2J_{HH}$ = 15.7 Hz, roofing diastereotopic PhCH_2), 7.03–7.27 (m, 7H, 4 × Ar-CH, *o*-Ph and *p*-Ph), 7.33 (m, 2H, *m*-Ph), 7.44 (dd, 1H, $^3J_{HH}$ = 8.6 Hz and w-coupling $^4J_{HH}$ = 2.0 Hz, Ar: –CH–C*H*–C(Cl)CH–), 7.71 (d, 1H, w-coupling $^4J_{HH}$ = 2.0 Hz, Ar: CH–C(Cl)–C*H*C(N)), 8.26 (d, 1H, $^3J_{HH}$ = 8.6 Hz, Ar: C–C*H*–CH–C(Cl)). ^{13}C{^{1}H} (100 MHz, $CDCl_3$): δ_C 18.4 (CH_3), 19.2 (CH_3), 28.4 (3 × CH_3), 29.0 ($CHCH(CH_3)_2$: HSQC), 31.1 (–$NCH_2CH_2CH_2$–), 37.7 (–$NCH_2CH_2CH_2$–), 42.2 (–$NCH_2CH_2CH_2$–), 45.6 (PhCH_2), 59.8 ($CHCH(CH_3)_2$), 79.5 (O$C(CH_3)_3$), 115.8 and 116.0 (2C, Ar: 2 × F-C*C*H), 119.4 (IV° C), 126.9 (Ar: CH–C(Cl)–*C*HC(N)), 127.3 (2 × *o*-Ph), 127.8 (*p*-Ph), 128.2 (Ar: –CH–*C*H–C(Cl)CH–), 128.3 (2C, Ar: 2 × F-CC*H*CH), 128.9 (2 × *m*-Ph), 129.0 (Ar: –*C*H–CH–C(Cl)CH), 136.8 (IV° C), 141.0 (IV° C), 147.6 (IV° C), 155.8 (IV° C), 161.9 (IV° C), 162.2 (IV° C), 164.4 (IV° C), 172.0 (IV° C). ^{19}F NMR (376 MHz, $CDCl_3$; $CFCl_3$ reference): δ_F −110.10 ppm. MS *m*/*z* (MeCN) 621 (100%) [M+H$^+$]. HRMS-ESI *m*/*z* (DCM/MeOH) found 621.2638, calcd for $C_{34}H_{39}ClFN_4O_4$ 621.2638 [M+H$^+$]. $[\alpha]_D$ (25 °C; $CHCl_3$; **15-(*R*)**) = +249.9 ± 0.7. Analytical data for the synthesis of racemate **15** and **15-(*S*)** were identical.

4.1.3. (±)-*tert*-Butyl (3-(*N*-(1-(3-benzyl-7-chloro-4-oxo-3,4-dihydroquinazolin-2-yl)-2-methylpropyl)-3-fluorobenzamido) propyl)carbamate 16

Compound **13** (0.10 g, 0.20 mmol) was reacted with *m*-fluorobenzoyl chloride (0.044 g, 0.28 mmol, 1.4 equiv) in accordance with general method A to give compound **16** (0.079 g, 0.127 mmol, 63%). ^{1}H NMR (400 MHz, $CDCl_3$): δ_H 0.37 (d, 3H, $^3J_{HH}$ = 6.4 Hz, magnetically inequivalent CH(CH_3)$_2$), 0.78 (m, 1H, –$CH_2CH_2CH_2$ diastereotopic), 0.95 (d, 3H, $^3J_{HH}$ = 6.7 Hz, magnetically inequivalent CH(CH_3)$_2$), 1.31 (m, 1H, –$CH_2CH_2CH_2$ diastereotopic), 1.41 (s, 9H, –OC(CH_3)$_3$), 2.59–2.79 (m, 3H, overlapping resonances: 1H, $CH_2CH(CH_3)_2$, and 2H, $NCH_2CH_2CH_2$–), 3.29–3.53 (m, 2H, $NCH_2CH_2CH_2$–, diastereotopic), 3.94 (br s, 1H, NHC(O)), 5.8 (d, 1H, $^2J_{HH}$ = 15.7 Hz, roofing diastereotopic PhCH_2), 5.68 (d, 1H, $^3J_{HH}$ = 10.5 Hz, $CHCH(CH_3)_2$), 6.12 (d, 1H, $^2J_{HH}$ = 15.7 Hz, roofing diastereotopic PhCH_2), 6.97–7.42 (m, 9H, Ar), 7.49 (dd, 1H, $^3J_{HH}$ = 8.6 Hz and w-coupling $^4J_{HH}$ = 1.8 Hz, Ar: –CH–C*H*–C(Cl)CH–), 7.76 (d, 1H, w-coupling $^4J_{HH}$ = 1.8 Hz, Ar: CH–C(Cl)–C*H*C(N)), 8.32 (d, 1H, $^3J_{HH}$ = 8.6 Hz, Ar: C–C*H*–CH–C(Cl)). ^{13}C{^{1}H} (100 MHz, $CDCl_3$): δ_C 18.4 (CH_3), 19.2 (CH_3), 28.5 (3 × CH_3), 29.0 ($CHCH(CH_3)_2$), 31.2 (–$NCH_2CH_2CH_2$–), 37.7 (–$NCH_2CH_2CH_2$–), 42.2 (–$NCH_2CH_2CH_2$–), 45.7 (PhCH_2), 59.8 ($CHCH(CH_3)_2$), 79.3 (O$C(CH_3)_3$ [weak]), 113.5 and 113.7 (1C, $^3J_{HF}$ = 23.0 Hz, Ar), 116.7 and 116.9 (1C, $^3J_{HF}$ = 20.8 Hz, Ar), 119.5 (IV° C), 121.8 (Ar), 127.0 (Ar:

CH–C(Cl)–CHC(N)), 127.3 (2 × *o*-Ph), 127.9 (*p*-Ph), 128.4 (Ar: –CH–CH–C(Cl)CH–), 128.9 (2 × *m*-Ph), 129.1 (Ar: –CH–CH–C(Cl)CH), 130.7 and 130.8 (1C, $^3J_{HF}$ = 8.0 Hz, Ar), 136.8 (IV° C), 138.6 and 138.7 (1C, $^3J_{HF}$ = 6.9 Hz, IV° C), 141.1 (IV° C), 147.7 (IV° C), 155.8 (IV° C), 161.3 (IV° C), 162.2 (IV° C), 163.8 (IV° C), 171.5 (IV° C). ^{19}F NMR (376 MHz, $CDCl_3$; $CFCl_3$ reference): δ_F −110.78 ppm. MS *m*/*z* (MeCN) 621 (100%) [M+H$^+$]. HRMS-ESI *m*/*z* (DCM/MeOH) found 621.2645, calcd for $C_{34}H_{39}ClFN_4O_4$ 621.2638 [M+H$^+$]. Analytical data for the synthesis of **16-(*R*)** and **16-(*S*)** were identical

4.1.4. (±)-*tert*-Butyl (3-(*N*-(1-(3-benzyl-7-chloro-4-oxo-3,4-dihydroquinazolin-2-yl)-2-methylpropyl)-2-fluorobenzamido) propyl)carbamate 17

Compound **13** (0.10 g, 0.20 mmol) was reacted with *o*-fluorobenzoyl chloride (0.044 g, 0.28 mmol, 1.4 equiv) in accordance with general method A to give compound **17** (0.110 g, 0.177 mmol, 89%). ^{1}H NMR (400 MHz, $CDCl_3$): δ_H 0.38 (d, 3H, $^3J_{HH}$ = 6.3 Hz, magnetically inequivalent CH(CH_3)$_2$), 0.77 (m, 1H, –$CH_2CH_2CH_2$ diastereotopic), 0.96 (d, 3H, $^3J_{HH}$ = 6.8 Hz, magnetically inequivalent CH(CH_3)$_2$), 1.41 (br s, 10H, overlapping 9H, –OC(CH_3)$_3$ and 1H, -$CH_2CH_2CH_2$ diastereotopic), 2.58–2.77 (m, 3H, overlapping resonances: 1H, $CH_2CH(CH_3)_2$, and 2H, $NCH_2CH_2CH_2$–), 3.23–3.52 (m, 2H, $NCH_2CH_2CH_2$–, diastereotopic), 3.95 (br s, 1H, NHC(O)), 5.13 (d, 1H, $^2J_{HH}$ = 15.7 Hz, roofing diastereotopic PhCH_2), 5.70 (d, 1H, $^3J_{HH}$ = 10.6 Hz, $CHCH(CH_3)_2$), 6.16 (d, 1H, $^2J_{HH}$ = 15.7 Hz, roofing diastereotopic PhCH_2), 7.12–7.42 (m, 9H, Ar), 7.49 (dd, 1H, $^3J_{HH}$ = 8.6 Hz and w-coupling $^4J_{HH}$ = 2.0 Hz, Ar: –CH–CH–C(Cl)CH–), 7.77 (d, 1H, w-coupling $^4J_{HH}$ = 2.0 Hz, Ar: CH–C(Cl)–CHC(N)), 8.33 (d, 1H, $^3J_{HH}$ = 8.6 Hz, Ar: C–CH–CH–C(Cl)). ^{13}C{^{1}H} (100 MHz, $CDCl_3$): δ_C 18.2 (CH_3), 19.2 (CH_3), 28.4 (3 × CH_3), 28.8 ($CHCH(CH_3)_2$), 30.7 (–$NCH_2CH_2CH_2$–), 37.7 (–$NCH_2CH_2CH_2$–), 41.8 (-$NCH_2CH_2CH_2$-), 45.6 (PhCH_2), 59.8 ($CHCH(CH_3)_2$), 79.4 (O$C(CH_3)_3$ [weak]), 116.2 and 116.4 (1C, $^3J_{HF}$ = 20.9 Hz, Ar), 119.4 (IV° C), 124.69 and 124.72 (1C, $^3J_{HF}$ = 3.1 Hz, Ar), 124.8 and 125.0 (1C, $^3J_{HF}$ = 18.4 Hz, Ar), 126.9 (Ar: CH–C(Cl)–CHC(N)), 127.3 (2 × *o*-Ph), 127.8 (*p*-Ph), 128.3 (Ar: –CH–CH–C(Cl)CH–), 128.8 (2 × *m*-Ph), 129.0 (Ar: –CH–CH–C(Cl)CH), 131.3 and 131.4 (1C, $^3J_{HF}$ = 7.7 Hz, Ar), 136.8 (IV° C), 140.9 (IV° C), 147.6 (IV° C), 155.7 (IV° C), 156.4 (IV° C), 158.9 (IV° C), 162.2 (IV° C), 168.4 (IV° C), 171.2 (IV° C). ^{19}F NMR (376 MHz, $CDCl_3$; $CFCl_3$ reference): δ_F −114.22 ppm. MS *m*/*z* (MeCN) 621 (100%) [M+H$^+$]. HRMS-ESI *m*/*z* (DCM/MeOH) found 621.2644, calcd for $C_{34}H_{39}ClFN_4O_4$ 621.2638 [M+H$^+$]. Analytical data for the synthesis of **17-(*R*)** and **17-(*S*)** were identical.

4.1.5. (*R*)-*tert*-Butyl (3-(*N*-(1-(3-benzyl-7-chloro-4-oxo-3,4-dihydroquinazolin-2-yl)-2-methylpropyl)-4-nitrobenzamido) propyl)carbamate 18

Compound **13-(*R*)** (0.150 g, 0.30 mmol) was reacted with *p*-nitrobenzoyl chloride (0.078 g, 0.42 mmol, 1.4 equiv) in accordance with general method A to give compound **18** (0.176 g, 0.272 mmol, 91%). ^{1}H NMR (400 MHz, $CDCl_3$): δ_H 0.39 (d, 3H, $^3J_{HH}$ = 6.4 Hz, magnetically inequivalent CH(CH_3)$_2$), 0.80 (m, 2H, –$CH_2CH_2CH_2$), 0.85 (d, 3H, $^3J_{HH}$ = 7.3 Hz, magnetically inequivalent CH(CH_3)$_2$), 1.38 (s, 9H, –OC(CH_3)$_3$), 2.55–2.81 (m, 3H, overlapping resonances: 1H, $CH_2CH(CH_3)_2$, and 2H, $NCH_2CH_2CH_2$–), 3.22–3.54 (m, 2H, $NCH_2CH_2CH_2$– diastereotopic), 4.00 (br s, 1H, NHC(O)), 5.17 (d, 1H, $^2J_{HH}$ = 15.8 Hz, roofing diastereotopic PhCH_2), 5.71 (d, 1H, $^3J_{HH}$ = 10.6 Hz, $CHCH(CH_3)_2$), 6.13 (d, 1H, $^2J_{HH}$ = 15.8 Hz, roofing diastereotopic PhCH_2), 7.28-7.45 (m, 7H, 2 × Ar-CH, *o*-Ph, m-Ph and *p*-Ph), 7.50 (dd, 1H, $^3J_{HH}$ = 8.6 Hz and w-coupling $^4J_{HH}$ = 2.2 Hz, Ar: –CH–CH–C(Cl)CH–), 7.77 (d, 1H, w-coupling $^4J_{HH}$ = 2.2 Hz, Ar: CH–C(Cl)–CHC(N)), 8.28 (d, 2H, $^3J_{HH}$ = 8.6 Hz, Ar), 8.33 (d, 1H, $^3J_{HH}$ = 8.6 Hz, Ar: C–CH–CH–C(Cl)). ^{13}C{^{1}H} (100 MHz, $CDCl_3$): δ_C 18.5 (CH_3), 19.2 (CH_3), 28.4 (3 × CH_3), 29.1 ($CHCH(CH_3)_2$: HSQC), 31.4 (–$NCH_2CH_2CH_2$–), 37.6 (–$NCH_2CH_2CH_2$–), 42.2 (–$NCH_2CH_2CH_2$–), 45.8 (PhCH_2), 59.8 ($CHCH(CH_3)_2$), 79.8 (O$C(CH_3)_3$), 119.5 (IV° C), 124.2 (2 × CH–$ArNO_2$), 127.0 (Ar: CH–C(Cl)–CHC(N)), 127.2 (2 × *o*-Ph), 127.3 (2 × CH–$ArNO_2$), 128.0 (*p*-Ph), 128.5 (Ar: –CH–CH–C(Cl)CH–), 129.0 (2 × *m*-Ph), 129.1 (Ar: –CH–CH–C(Cl)CH), 136.7 (IV° C), 141.1 (IV° C), 142.8 (IV° C), 147.6 (IV° C), 155.4 (IV° C), 162.2 (IV° C), 170.9 (IV° C). MS *m*/*z* (MeCN) 648 (100%) [M+H$^+$]. HRMS-ESI *m*/*z* (DCM/MeOH) found 648.2582, calcd for $C_{34}H_{39}ClN_5O_6$ 648.2583 [M+H$^+$]. Analytical data for the synthesis of **18-(*R*)** and **18-(*S*)** were identical.

4.1.6. General method B

Deprotection of BOC-protect derivatives of ispinesib was accomplished using a standard trifluoroacetic acid method. Details are presented for the synthesis of (±)-*N*-(3-aminopropyl)-*N*-(1-(3-benzyl-7-chloro-4-oxo-3,4-dihydroquinazolin-2-yl)-2-methylpropyl)-4-methylbenzamide, racemate **19** (ispinesib).

Compound **14** (0.139 g, 0.226 mmol) was added to a flame dried 25 ml round bottom flask, placed under N_2(g) atmosphere and dissolved in anhydrous dichloromethane (2 mL). Trifluoroacetic acid (TFA; 2 mL) was added and the reaction was stirred at rt for 2 h. The reaction was monitored by TLC (30% EtOAc/hexanes/∼0.1% conc. NH_3, UV) with the product observed as the major spot at the baseline R_f = 0.00 and the starting compound **14** at R_f = 0.50. Solvents were then removed under reduced pressure and the crude residue was dissolved in dichloromethane (20 mL), washed with sat. $NaHCO_3$(aq) (2 × 15 mL), brine (15 mL). The organic fraction was separated, dried over Na_2SO_4(s) for 30 min, filtered and then the solvent was removed under reduced pressure and the sample dried in vacuo to give purified compound **19**, (±)-ispinesib, as a white solid (0.105 g, 0.20 mmol, 88%). ^{1}H NMR (400 MHz, $CDCl_3$): δ_H 0.38 (d, 3H, $^3J_{HH}$ = 6.4 Hz, magnetically inequivalent CH(CH_3)$_2$), 0.81–0.88 (m, 1H, –$CH_2CH_2CH_2$ diastereotopic), 0.96 (d, 3H, $^3J_{HH}$ = 6.7 Hz, magnetically inequivalent CH(CH_3)$_2$), 1.32–1.33 (m, 1H, –$CH_2CH_2CH_2$ diastereotopic), 2.17–2.21 (m, 2H, $NCH_2CH_2CH_2$–), 2.36 (s, 3H, PhCH_3), 2.70–2.79 (m, 1H, $CH_2CH(CH_3)_2$), 3.35–3.50 (m, 2H, $NCH_2CH_2CH_2$–), 5.22 (d, 1H, $^2J_{HH}$ = 15.7 Hz, roofing diastereotopic PhCH_2), 5.71 (d, 1H, $^3J_{HH}$ = 10.6 Hz, $CHCH(CH_3)_2$), 6.11 (d, 1H, $^2J_{HH}$ = 15.7 Hz, roofing diastereotopic PhCH_2), 7.18–7.23 (m, 4H, 4 × Ar-CH, tolyl group), 7.27 (m, 2H, *o*-Ph overlapping with $CHCl_3$ residual solvent resonance), 7.31 (m, 1H, *p*-Ph), 7.40 (m, 2H, *m*-Ph), 7.46 (dd, 1H, $^3J_{HH}$ = 8.6 Hz and w-coupling $^4J_{HH}$ = 2.0 Hz, Ar: –CH–CH–C(Cl)CH–), 7.69 (d, 1H, w-coupling $^4J_{HH}$ = 2.0 Hz, Ar: CH–C(Cl)–CHC(N)), 8.30 (d, 1H, $^3J_{HH}$ = 8.6 Hz, Ar: C–CH–CH–C(Cl)) NB: NH_2 proton resonance was not observed. ^{13}C{^{1}H} (100 MHz, $CDCl_3$): δ_C 18.5 (CH_3), 19.3 (CH_3), 21.5 (PhCH_3), 29.0 ($CHCH(CH_3)_2$: HSQC), 33.4 (–$NCH_2CH_2CH_2$–), 39.3 (–$NCH_2CH_2CH_2$–), 42.3 (–$NCH_2CH_2CH_2$–), 45.7 (PhCH_2), 59.7 ($CHCH(CH_3)_2$), 119.5 (IV° C), 126.2 (2C, Ar: 2 × CH_3CHCH), 127.0 (Ar: CH–C(Cl)–CHC(N)), 127.4 (2 × *o*-Ph), 127.8 (*p*-Ph), 128.2 (Ar: –CH–CH–C(Cl)CH–), 128.9 (2C, Ar: 2 × CH_3CHCH: HMBC), 129.1 (Ar: –CH–CH–C(Cl)CH), 129.4 (2 × *m*-Ph), 134.0 (IV° C), 137.0 (IV° C), 139.7 (IV° C), 140.9 (IV° C), 147.8 (IV° C), 156.1 (IV° C), 162.4 (IV° C), 173.2 (IV° C). MS *m*/*z* (MeCN) 517 (100%) [M+H$^+$]. HRMS-ESI *m*/*z* (DCM/MeOH) found 517.2359, calcd for $C_{30}H_{34}ClN_4O_{42}$ 517.2365 [M+H$^+$]. $[\alpha]_D$ (25 °C; $CHCl_3$; **19-(*R*)**) = +345.9 ± 0.4. Analytical data for the synthesis of **19-(*R*)** and **19-(*S*)** were identical.

4.1.7. (±)-*N*-(3-aminopropyl)-*N*-(1-(3-benzyl-7-chloro-4-oxo-3,4-dihydroquinazolin-2-yl)-2-methylpropyl)-4-fluorobenzamide 20

Compound **15** (0.115 g, 0.185 mmol) was deprotected in accordance with general method B to give compound **20** as a white solid (0.078 g, 0.15 mmol, 81%). ^{1}H NMR (400 MHz, $CDCl_3$): δ_H 0.37 (d, 3H, $^3J_{HH}$ = 6.4 Hz, magnetically inequivalent CH(CH_3)$_2$), 0.86 (m, 1H, –$CH_2CH_2CH_2$ diastereotopic), 0.95 (d, 3H, $^3J_{HH}$ = 6.7 Hz,

magnetically inequivalent $CH(CH_3)_2$), 1.32 (m, 1H, $-CH_2CH_2CH_2$ diastereotopic), 2.22 (m, 2H, $NCH_2CH_2CH_2-$), 2.74 (m, 1H, $CH_2CH(CH_3)_2$), 3.33-3.53 (m, 2H, $NCH_2CH_2CH_2-$), 5.18 (d, 1H, $^2J_{HH}$ = 15.7 Hz, roofing diastereotopic $PhCH_2$), 5.70 (d, 1H, $^3J_{HH}$ = 10.5 Hz, $CHCH(CH_3)_2$), 6.11 (d, 1H, $^2J_{HH}$ = 15.7 Hz, roofing diastereotopic $PhCH_2$), 7.07–7.39 (m, 9H, 4 × Ar-CH, *o*-Ph, *m*-Ph and *p*-Ph), 7.47 (dd, 1H, $^3J_{HH}$ = 8.6 Hz and w-coupling $^4J_{HH}$ = 2.0 Hz, Ar: –CH–CH–C(Cl)CH–), 7.69 (d, 1H, w-coupling $^4J_{HH}$ = 2.0 Hz, Ar: CH–C(Cl)–CHC(N)), 8.29 (d, 1H, $^3J_{HH}$ = 8.6 Hz, Ar: C–CH–CH–C(Cl)). $^{13}C\{^1H\}$ (100 MHz, $CDCl_3$): δ_C 18.5 (CH_3), 19.3 (CH_3), 29.1 ($CHCH(CH_3)_2$: HSQC), 32.6 ($-NCH_2CH_2CH_2-$), 39.0 ($-NCH_2CH_2CH_2NH_2$), 42.3 ($-NCH_2CH_2CH_2NH_2$), 45.7 ($PhCH_2$), 59.9 ($CHCH(CH_3)_2$), 115.9 and 116.1 (2C, Ar: 2 × F-CCH), 119.5 (IV° C), 127.0 (Ar: CH–C(Cl)–CHC(N)), 127.3 (2 × *o*-Ph), 127.9 (*p*-Ph), 128.3 and 128.35 (2C, Ar: 2 × F-CCHCH), 128.4 (Ar: –CH–CH–C(Cl)CH–), 128.9 (2 × *m*-Ph), 129.1 (Ar: –CH–CH–C(Cl)CH), 132.9 (IV° C), 136.9 (IV° C), 141.0 (IV° C), 147.7 (IV° C), 155.8 (IV° C), 162.3 (IV° C), 164.4 (IV° C), 172.1 (IV° C). ^{19}F NMR (376 MHz, $CDCl_3$; $CFCl_3$ reference): δ_F −110.28 ppm. MS *m*/*z* (MeCN) 521 (100%) $[M+H^+]$. HRMS-ESI *m*/*z* (DCM/MeOH) found 521.2105, calcd for $C_{29}H_{31}ClFN_4O_2$ 521.2114 $[M+H^+]$. $[\alpha]_D$ (25 °C; $CHCl_3$; **20-(*R*)**) = +306.4 ± 0.8. Analytical data for the synthesis of **20-(*R*)** and **20-(*S*)** were identical.

4.1.8. (±)-*N*-(3-Aminopropyl)-*N*-(1-(3-benzyl-7-chloro-4-oxo-3,4-dihydroquinazolin-2-yl)-2-methylpropyl)-3-fluorobenzamide 21

Compound **16** (0.079 g, 0.127 mmol) was deprotected in accordance with general method B to give compound **21** as a white solid (0.053 g, 0.102 mmol, 80%). ^1H NMR (400 MHz, $CDCl_3$): δ_H 0.39 (d, 3H, $^3J_{HH}$ = 6.4 Hz, magnetically inequivalent $CH(CH_3)_2$), 0.85 (m, 1H, $-CH_2CH_2CH_2$ diastereotopic), 0.95 (d, 3H, $^3J_{HH}$ = 6.8 Hz, magnetically inequivalent $CH(CH_3)_2$), 1.30 (m, 1H, $-CH_2CH_2CH_2$ diastereotopic), 2.22 (m, 2H, $NCH_2CH_2CH_2-$), 2.76 (m, 1H, $CH_2CH(CH_3)_2$), 3.43 (m, 2H, $NCH_2CH_2CH_2-$), 5.17 (d, 1H, $^2J_{HH}$ = 15.6 Hz, roofing diastereotopic $PhCH_2$), 5.70 (d, 1H, $^3J_{HH}$ = 10.6 Hz, $CHCH(CH_3)_2$), 6.13 (d, 1H, $^2J_{HH}$ = 15.6 Hz, roofing diastereotopic $PhCH_2$), 7.02-7.40 (m, 9H, 4 × Ar-CH, *o*-Ph, *m*-Ph and *p*-Ph), 7.48 (dd, 1H, $^3J_{HH}$ = 8.6 Hz and w-coupling $^4J_{HH}$ = 2.0 Hz, Ar: –CH–CH–C(Cl)CH–), 7.69 (d, 1H, w-coupling $^4J_{HH}$ = 2.0 Hz, Ar: CH–C(Cl)–CHC(N)), 8.30 (d, 1H, $^3J_{HH}$ = 8.6 Hz, Ar: C–CH–CH–C(Cl)). ^{19}F NMR (376 MHz, $CDCl_3$; $CFCl_3$ reference): δ_F -111.3 ppm. MS *m*/*z* (MeCN) 521 (100%) $[M+H^+]$. HRMS-ESI *m*/*z* (DCM/MeOH) found 521.2099, calcd for $C_{29}H_{31}ClFN_4O_2$ 521.2114 $[M+H^+]$. $[\alpha]_D$ (25 °C; $CHCl_3$; **21-(*S*)**) = −339.7 ± 0.8. Analytical data for the synthesis of **21-(*R*)** and **21-(*S*)** were identical.

4.1.9. (±)-*N*-(3-Aminopropyl)-*N*-(1-(3-benzyl-7-chloro-4-oxo-3,4-dihydroquinazolin-2-yl)-2-methylpropyl)-2-fluorobenzamide 22

Compound **17** (0.107 g, 0.172 mmol) was deprotected in accordance with general method B to give compound **22** as a white solid(0.073 g, 0.140 mmol, 81%). ^1H NMR (400 MHz, $CDCl_3$): δ_H 0.39 (d, 3H, $^3J_{HH}$ = 6.4 Hz, magnetically inequivalent $CH(CH_3)_2$), 0.83 (m, 1H, $-CH_2CH_2CH_2$ diastereotopic), 0.96 (d, 3H, $^3J_{HH}$ = 6.8 Hz, magnetically inequivalent $CH(CH_3)_2$), 1.26 (m, 1H, $-CH_2CH_2CH_2$ diastereotopic), 2.18 (m, 2H, $NCH_2CH_2CH_2-$), 2.75 (m, 1H, $CH_2CH(CH_3)_2$), 3.38 (m, 2H, $NCH_2CH_2CH_2-$), 5.11 (d, 1H, $^2J_{HH}$ = 15.7 Hz, roofing diastereotopic $PhCH_2$), 5.70 (d, 1H, $^3J_{HH}$ = 10.6 Hz, $CHCH(CH_3)_2$), 6.13 (d, 1H, $^2J_{HH}$ = 15.7 Hz, roofing diastereotopic $PhCH_2$), 7.10–7.41 (m, 9H, 4 × Ar-CH, *o*-Ph, *m*-Ph and *p*-Ph), 7.48 (dd, 1H, $^3J_{HH}$ = 8.6 Hz and w-coupling $^4J_{HH}$ = 2.0 Hz, Ar: –CH–CH–C(Cl)CH–), 7.69 (d, 1H, w-coupling $^4J_{HH}$ = 2.0 Hz, Ar: CH–C(Cl)–CHC(N)), 8.31 (d, 1H, $^3J_{HH}$ = 8.6 Hz, Ar: C–CH–CH–C(Cl)). ^{19}F NMR (376 MHz, $CDCl_3$; $CFCl_3$ reference): δ_F −114.71 ppm. MS *m*/*z* (MeCN) 521 (100%) $[M+H^+]$. HRMS-ESI *m*/*z* (DCM/MeOH) found 521.2115, calcd for $C_{29}H_{31}ClFN_4O_2$ 521.2114 $[M+H^+]$. $[\alpha]_D$ (25 °C; $CHCl_3$; **22-(*S*)**) = −355.6 ± 0.4. Analytical data for the synthesis of **22-(*R*)** and **22-(*S*)** were identical.

4.1.10. Mosher's amide synthesis

The absolute configuration of the stereo-center in chirally resolved compound **10-(*R*)** was assigned by synthesising the Mosher's amide derivatives **23-(*R*,*R*)** and **23-(*R*,*S*)** in accordance with the methods described by Hoye et al.[18,22]

4.1.11. Synthesis of compound 23-(*R*,*R*)

*NB: The absolute configuration of the stereo-center in resolved compound **10-(R)** was not known prior to Mosher's amide analysis.* Compound numbers are given here for clarity and reflect the results of this analysis. To a 10 mL reaction vial was added compound **10-(*R*)** (0.025 g, 7.3×10^{-5} mol), (*R*)-(+)-α-methoxy-α-trifluoromethylphenyl acetic acid (*R*-(+)-MTPA-OH; 0.0553 g, 2.36×10^{-4} mol, 3.23 equiv), anhydrous pyridine (.023 g, 2.9×10^{-4} mol, 4 equiv) in anhydrous dichloromethane (total of 1.0 mL). Then *N*,*N*′-dicyclohexylcarbodiimide (DCC; 0.060 g, 2.9×10^{-4} mol, 4 equiv) was added at rt with stirring upon which a white precipitate formed immediately. The reaction was left to stir at rt for 24 h and monitored by TLC (20% EtOAc/hexanes, UV) with the product observed as the major spot at R_f = 0.40. Then the reaction was filtered through a cotton plug to remove the insoluble dicyclohexylurea (DCU) by-product before partitioning the filtrate between water (5 mL) and diethyl ether (10 mL). The mixture was separated and the aqueous fraction was extracted with diethyl ether (3 × 10 mL). The organic fractions were combined, dried over anhydrous Na_2SO_4(s) for 30 min, filtered and then the solvent was removed under reduced pressure. The crude mixture was purified on a small silica gel column (15% EtOAc/hexane), fractions containing product were identified by TLC, pool and dried the solvent was removed under reduced pressure. The final compound was dried in vacuo to give compound **23-(*R*,*R*)** as a clear light pink coloured oil (0.0318 g, 5.7×10^{-5} mol, 78%). *NB: Only selected NMR data used in the analysis of the absolute configuration are presented. Resonance assignments correspond with those listed in* Scheme 2. ^1H NMR (400 MHz, $CDCl_3$): δ_H 0.385 (d, 3H, $^3J_{HH}$ = 6.7 Hz, magnetically inequivalent $CH(CH_3)_2$ [a]), 0.736 (d, 3H, $^3J_{HH}$ = 6.7 Hz, magnetically inequivalent $CH(CH_3)_2$ [a*]), 2.09 (m, 1H, $CH_2CH(CH_3)_2$ [b]), 5.16 (m, 1H, $CHCH(CH_3)_2$ [c]), 5.28 (d, 1H, $^2J_{HH}$ = 15.7 Hz, roofing diastereotopic $PhCH_2$ [g]), 5.81 (d, 1H, $^2J_{HH}$ = 15.7 Hz, roofing diastereotopic $PhCH_2$ [g*]), 8.28 (d, 1H, $^3J_{HH}$ = 8.6 Hz, Ar: C-CH-CH-C(Cl) [f]). MS *m*/*z* (MeCN) 558 (100%) $[M+H^+]$. HRMS-ESI *m*/*z* (DCM/MeOH) found 558.1771, calcd for $C_{29}H_{28}ClF_3N_3O_3$ 558.1766 $[M+H^+]$.

4.1.12. Synthesis of compound 23-(*R*,*S*)

With the exception of using (*S*)-(−)-α-methoxy-α-trifluoromethylphenyl acetic acid, *S*-(−)-MTPA-OH, the same procedure given for the synthesis of compound **23-(*R*,*R*)** was used to give compound **23-(*R*,*S*)** as a clear light pink coloured oil (0.041 g, 7.35×10^{-5} mol, 100%). ^1H NMR (400 MHz, $CDCl_3$): δ_H 0.44 (d, 3H, $^3J_{HH}$ = 6.2 Hz, magnetically inequivalent $CH(CH_3)_2$ [a]), 0.91 (d, 3H, $^3J_{HH}$ = 6.4 Hz, magnetically inequivalent $CH(CH_3)_2$ [a*]), 2.14 (m, 1H, $CH_2CH(CH_3)_2$ [b]), 5.13 (m, 1H, $CHCH(CH_3)_2$ [c]), 5.29 (d, 1H, $^2J_{HH}$ = 15.6 Hz, roofing diastereotopic $PhCH_2$ [g]), 5.77 (d, 1H, $^2J_{HH}$ = 15.6 Hz, roofing diastereotopic $PhCH_2$ [g*]), 8.27 (d, 1H, $^3J_{HH}$ = 8.6 Hz, Ar: C-CH-CH-C(Cl) [f]). MS *m*/*z* (MeCN) 558 (100%) $[M+H^+]$. HRMS-ESI *m*/*z* (DCM/MeOH) found 558.1772, calcd for $C_{29}H_{28}ClF_3N_3O_3$ 558.1766 $[M+H^+]$.

4.2. Single-crystal X-ray diffraction

Single crystal X-ray diffraction data were obtained for compounds **3**, **7** and **9**. In each case, a typical crystal was mounted

using the oil drop technique, in perfluoropolyether oil at 150(2) K using a Cryostream N_2 open-flow cooling device.[23] Diffraction data were collected using graphite monochromatic Mo-K_α radiation (λ = 0.71073 Å) on a Nonius Kappa CCD diffractometer. For all data collections, series of ω-scans were performed in such a way as to collect a complete data set to a maximum resolution of 0.77 Å. Data reduction including unit cell refinement and inter-frame scaling was carried out using DENZO-SMN/SCALEPACK.[24] Intensity data were processed and corrected for absorption effects by the multi-scan method, based on repeat measurements of identical and Laue equivalent reflections. Structure solution was carried out with direct methods using the program SIR92[25] within the CRYSTALS software suite.[26] In general, coordinates and anisotropic displacement parameters of all non-hydrogen atoms were refined freely except where disorder necessitated the use of "same distance restraints" together with thermal similarity and vibrational restraints to maintain sensible geometry/displacement parameters. Hydrogen atoms were generally visible in the difference map and refined with soft restraints prior to inclusion in the final refinement using a riding model.[27] Crystallographic data (excluding structure factors) for all the structures have been deposited with the Cambridge Crystallographic Data Centre (CCDC: 897765–897767). Copies of these data can be obtained free of charge from The Cambridge Crystallographic Data Centre via www.ccdc.cam.ac.uk/data_request/cif. A summary of the X-ray crystallographic data is provided in Supplementary data Table S1.

4.3. Kinesin motor protein ATP-hydrolase inhibition assay

Inhibition of the ATP-hydrolase activity of various kinesin motor proteins was measured by using the Kinesin ATPase End-Point Biochem Kit, BK053 (Cytoskeleton, Denver, USA). All motor proteins were also obtained from Cytoskeleton. Generation of inorganic phosphate (Pi) during MT-activated ATP-hydrolase activity of kinesin motor proteins was measured at 650 nm. The concentration of the motor proteins (2.5 μg total protein) used in the assay was kept as low as possible to minimise possible crowding effects on MTs. Compounds were diluted to give final concentrations of 1.0 μM and were incubated at rt for 10 to 20 min. Assays were conducted in accordance with the manufacturer's protocol.

4.4. Cells and cell culture

Cell culture media and additives were obtained from BioConcept (Allschwil, Switzerland). PC-3 human prostate adenocarcinoma and SKOV3 human ovary adenocarcinoma cells were obtained from the European Collection of Cell Cultures (ECACC, Salisbury, UK) and were maintained in Dulbecco's Modified Eagle's Medium (DMEM) with 10% Fetal Calf Serum (FCS) (v/v). DU-145 human prostate carcinoma cells were cultured in Minimum Essential Medium Eagle (MEM) containing sodium pyruvate (1 mM), sodium bicarbonate (1.5 g/L) and 1% non-essential amino acids (NEAA). MCF-7 human breast cancer epithelial cells were cultured in a 1:1 mixture of DMEM/Ham's F-12 medium. All cell culture media were supplemented with 10% (v/v) fetal calf serum (FCS), glutamine (2 mM), and antibiotics (penicillin [100 units/mL], streptomycin [100 μg/mL] and fungizone [0.25 μg/mL]). All cell lines were maintained at 37 °C with 5% carbon dioxide.

4.5. In vitro cell proliferation assays

Compounds were dissolved in DMSO in concentrations ranging from 1.0 to 1.0 mM. The compounds were serially diluted (typically 1:4 or 1:2 dilution) with growth medium then diluted into the cell assay plate with a final DMSO concentration of $\leqslant$0.2%. Cells were plated in 96-well plates with a density of 2000 cells/well with the exception of MCF-7, where cell density was 1000 cells/well, and allowed to adhere for 24 h. Cells were then exposed to the compounds which were added directly to the media. Appropriate controls for culture media and vehicle were used throughout to measure non-specific background, and to serve as a reference to each cell line. Plates were incubated at 37 °C for 44 h then treated with MTT solution and cultured for 3 h. After removing the media, DMSO (100 μL/well) was added to solubilise the purple formazan product. Absorbance was then measured at 560 nm by using Perkin Elmer Victor™ X3 Multilabel Plate Reader. Dose–response curves following either a monophasic or biphasic profile were determined with GraphPad Prism 5.01 (GraphPad Software, La Jolla, CA, USA) by non-linear regression analysis of a plot of absorbance (560 nm) versus drug concentration.

BrdU assays were conducted in a similar manner to the MTT assays and were analysed by using the Cell Proliferation ELISA BrdU assay kit (Roche Applied Science, Mannheim, Germany) in accordance with the manufacturer's protocol.

4.6. Flow cytometry

Cells were plated onto 100 mm^2 dishes at a cell density of 1.0×10^6 cells/dish and 24 h later, were treated with 100 nM of the compounds. 24 h after treatment, cells were washed once with ice-cold PBS (5 mL), detached by treatment with trypsin/EDTA solution and centrifuged for 5 min at 1000 rpm at rt. The cell pellet was washed twice with 10 mL PBS, resuspended in 4 mL of ice-cold fixation solution (70 vol% ethanol, 30 vol% H_2O) and stored at −20 °C for 24 h. Thereafter, cold PBS (10 mL) was added to the cell suspension before centrifugation for 5 min at 1000 rpm. The cell pellet was washed once with PBS (10 mL; 4 °C) and resuspended in 1.0 mL of staining solution containing 0.1 mg/mL RNAse A (Sigma Aldrich), 50 μg/mL propidium iodide (PI) from 2.5 mg/mL stock solution and 0.05% Triton X-100 (Fluka) in PBS. After incubation at 37 °C for 40 min in the dark, cells were washed in PBS, and analysed on a guava easyCyte HT2L flow cytometry system (Millipore). Data were analysed by cell-cycle analysis software (Flowjo, Tree-Star Inc.). For phospho-histone H3 analysis, fixed cells were incubated with a mouse anti-phospho-histone H3 (Ser10) antibody (1:50 dilution in PBS, Cell Signalling Technology, BioConcept, Allschwil, Switzerland) for 45 min at rt. The cells were washed twice with PBS and incubated with a FITC-conjugated goat anti-mouse IgG (1:200 dilution in PBS, Sigma–Aldrich, Buchs, Switzerland) for 30 min in the dark. Cells were stained with PI as described above before flow cytometric analysis.

4.7. Confocal fluorescence microscopy

4.7.1. Permeabilisation buffer

Permeabilisation buffer was freshly prepared from a 10× concentrated stock solution (1.54 M NaCl, 15.44 mM KH_2PO_4, 28.58 mM $Na_2HPO_4{\cdot}7H_2O$ and 5% Triton X-100). To 10× permeabilisation buffer (5 mL) was added deionised H_2O (40 mL). The pH was adjusted to pH 7.2, and then the solution was diluted to 50 mL to make a 1.0× permeabilisation buffer stock solution. Stock solutions can be kept for several weeks in a refrigerator. To 1.0× permeabilisation buffer (2.4 mL) was added PBS (9.6 mL) to give 0.2× permeabilisation buffer used as working solution.

4.7.2. Blocking buffer

A solution of PBS containing 1% BSA and 0.3% Tween-20 was prepared.

4.7.3. Confocal fluorescence microscopy

Cells were maintained at 37 °C with 5% carbon dioxide and were plated in 8-well Lab-Tek II Chamber Slides (NUNC, VWR, LabShop,

Batavia, IL) with a density of 5000 cells/well and allowed to adhere for 24 h and to grow to 80% confluence. Cells were then exposed to 0.1 μM concentrations of compounds **20**–**22** and incubated for 22 h at 37 °C. All plates contained wells with culture media only to serve as a reference control to the SKOV-3 cell line.

Cells were washed with PBS (3 × 400 μL), incubated with freshly prepared, pre-warmed 4% paraformaldehyde (400 μL) for 15 min at 37 °C, washed with PBS (3 × 400 μL), incubated with a freshly made 0.2× permeabilisation buffer (300 μL) for 15 min at 37 °C, washed with PBS (3 × 400 μL), incubated with 1 drop of ImageitFX (Invitrogen 'Signal Enhancer') for 30 min, washed with PBS (3 × 400 μL) and incubated with primary antibody (250 μL, Mouse α-tubulin [1:1000 dilution in blocking buffer; Sigma Aldrich]) at 37 °C for 2 h. Then cells were washed with PBS (3 × 400 μL), incubated with secondary antibody (250 μL, Goat a-Mouse Alexa Fluor 568 α-tubulin staining [Invitrogen], 1:2000 dilution in blocking buffer) at 37 °C for 1.5 h then washed with PBS (3 × 400 μL), incubated with Hoechst 33342 1:100,000 in deionised H_2O (2 μM) for 10 min and finally washed with deionised H_2O (3 × 400 μL). Slides were drained and all areas surrounding the tissue were dried then mounted onto microscope slides with one drop of Prolong Gold (Invitrogen), sealed with nail polish (Gemey, Express Finish) and kept in the dark at 4 °C.

Images were captured using a Zeiss LSM 510 laser scanning confocal microscope, 63× oil DIC Plan-Apochromat objective, 1.4NA. The microscope was incubated in an EMBL incubator box GP 168 at 36.5 °C. Solid state (561 nm) and Diode (405–430 nm) laser lines were used to image Alexa 568 α-tubulin staining and Hoechst 33342, respectively. Images were processed using AIM LSM4.0 software (Carl Zeiss) and ImageJ (National Institutes of Health, USA).

Acknowledgments

Funded in part by the ETH Fellowship Program (FEL-01-10-1; JPH). We thank Dr. NagaVaraKishore Pillarsetty, Dr. Aristeidis Chiotellis, Dr. Selena Melicevic Sephton and Cindy Fischer for helpful discussions and advice regarding chemical synthesis and chromatography. We also thank Dr. Tobias Schwarz and Dr. Joaquim Hehl at the Light Microscopy Centre, ETH Zurich for technical support regarding fluorescence microscopy studies.

A. Supplementary data

Supplementary data associated with this article can be found, in the online version, at http://dx.doi.org/10.1016/j.bmc.2012.11.013.

References and notes

1. Schmidt, M.; Bastians, H. *Drug Resist. Updates* **2007**, *10*, 162.
2. Yap, T. A.; Molife, L. R.; Blagden, S. P.; de Bono, S. *Exp. Opin. Drug Discovery* **2007**, *2*, 539.
3. Sharp, D. J.; Rogers, G. C.; Scholey, J. M. *Nature* **2000**, *407*, 41.
4. Carter, N. J.; Cross, R. A. *Nature* **2005**, *435*, 308.
5. Slangy, A.; Lane, H. A.; d'Hérin, P.; Harper, M.; Kress, M.; Niggt, E. A. *Cell* **1995**, *83*, 1159.
6. Weil, D.; Garçon, L.; Harper, M.; Duménil, M.; Dautry, F.; Kress, M. *Biotechniques* **2002**, *33*, 1244.
7. Tarby, C. M.; Kaltenbach, R. F., III; Huynh, T.; Pudzianowski, A.; Shen, H.; Ortega-Nanos, M.; Sheriff, S.; Newitt, J. A.; McDonnell, P. A.; Burford, N.; Fairchild, C. R.; Vaccaro, W.; Chen, Z.; Borzilleri, R. M.; Naglich, J.; Lombardo, L. J.; Gottardis, M.; Trainor, G. L.; Roussell, D. L. *Bioorg. Med. Chem. Lett.* **2006**, *16*, 2095.
8. Mayer, T. U.; Kapoor, T. M.; Haggarty, S. J.; King, R. W.; Schreiber, S. L.; Mitchison, T. J. *Science* **1999**, *286*, 971.
9. Sakowicz, R.; Finer, J. T.; Beraud, C.; Crompton, A.; Lewis, E.; Fritsch, A.; Lee, Y.; Mak, J.; Moody, R.; Turincio, R.; Chabala, J. C.; Gonzales, P.; Roth, S.; Weitman, S.; Wood, K. W. *Cancer Res.* **2004**, *64*, 3276.
10. Maliga, Z.; Kapoor, T. M.; Mitchison, T. J. *Chem. Biol.* **2002**, *9*, 989.
11. Maliga, Z.; Mitchison, T. *BMC Chem. Biol.* **2006**, *6*, 2.
12. Purcell, J. W.; Davis, J.; Reddy, M.; Martin, S.; Samayoa, K.; Vo, H.; Thomsen, K.; Bean, P.; Kuo, W. L.; Ziyad, S.; Billig, J.; Feiler, H. S.; Gray, J. W.; Wood, K. W.; Cases, S. *Clin. Cancer Res.* **2010**, *16*, 566.
13. DeBonis, S.; Skoufias, D. A.; Lebeau, L.; Lopez, R.; Robin, G.; Margolis, R. L.; Wade, R. H.; Kozielski, F. *Mol. Cancer Ther.* **2004**, *1079*, 3.
14. Zhang, B.; Liu, J.-F.; Xu, Y.; Ng, S.-C. *Biochem. Biophys. Res. Commun.* **2008**, *372*, 565.
15. Lad, L.; Luo, L.; Carson, J. D.; Wood, K. W.; Hartman, J. J.; Copeland, R. A.; Sakowicz, R. *Biochemistry* **2008**, *47*, 3576.
16. Miller, P. W.; Long, N. J.; Vilar, R.; Gee, A. D. *Angew. Chem., Int. Ed.* **2008**, *47*, 8998.
17. Tang, G.; Zeng, W.; Yu, M.; Kabalka, G. *J. Labelled Compd. Radiopharm.* **2008**, *51*, 68.
18. Hoye, T. R.; Jeffrey, C. S.; Shao, F. *Nat. Protoc.* **2007**, *2*, 2451.
19. Veras, E.; Malpica, A.; Deavers, M. T.; Silva, E. G. *Int. J. Gynecol. Pathol.* **2009**, *28*, 316.
20. Luo, L.; Parrish, C. A.; Nevins, N.; McNulty, D. E.; Chaudhari, A. M.; Carson, J. D.; Sudakin, V.; Shaw, A. N.; Lehr, R.; Zhao, H.; Sweitzer, S.; Lad, L.; Wood, K. W.; Sakowicz, R.; Annan, R. S.; Huang, P. S.; Jackson, J. R.; Dhanak, D.; Copeland, R. A.; Auger, K. R. *Nat. Chem. Biol.* **2007**, *3*, 722.
21. Sablin, E. P. *Curr. Opin. Cell Biol.* **2000**, *12*, 35.
22. Hoye, T. R.; Renner, M. K. *J. Org. Chem.* **1996**, *61*, 8489.
23. Cosier, J.; Glazer, A. M. *J. Appl. Crystallogr.* **1986**, *19*, 105.
24. Otwinowski, Z.; Minor, W. *Macromol. Crystallogr. Part A* **1997**, *276*, 307.
25. Altomare, A.; Cascarano, G.; Giacovazzo, C.; Guagliardi, A. *J. Appl. Crystallogr.* **1994**, *1045*, 27.
26. Watkin, D.; Cooper, R.; Prout, C. K. *Z Kristallographie* **2002**, *217*, 429.
27. Cooper, R. I.; Thompson, A. L.; Watkin, D. J. *J. Appl. Crystallogr.* **2010**, *43*, 1100.